3

Physics with BABAR

3.1 Physics Context

The study of *CP* violation in B decays is the primary physics objective of BaBar [SLA89]. The aim is to achieve a sufficient number of independent determinations of the parameters of the Cabibbo-Kobayashi-Maskawa (CKM) matrix to overdetermine those quantities. This then provides a test of the Standard Model interpretation of *CP* violation and, perhaps, a window into physics beyond the Standard Model [Nir93]. This chapter summarizes the essential physics points of this endeavor and briefly discusses other physics that can be done with BaBar. The measurement of *CP* violation asymmetries puts stringent requirements on the detector, so optimizing it for this purpose means that it is also well suited to study most of the other physics of interest in this energy regime.

The two mass eigenstates of the neutral B meson system can be written as:

$$\begin{aligned} |B_L\rangle &= p\,|B^0\rangle + q\,|\overline{B}^0\rangle, \\ |B_H\rangle &= p\,|B^0\rangle - q\,|\overline{B}^0\rangle, \end{aligned} \tag{3.1}$$

where H and L stand for Heavy and Light, respectively. Defining $M \equiv (M_H{+}M_L)/2$, $\Delta M \equiv M_H - M_L$, and neglecting the tiny difference in width between B_H and B_L, the decay widths satisfy $\Gamma_H = \Gamma_L \equiv \Gamma$. In this approximation, mixing in the B_d^0 system is governed by a single phase:

$$\left(\frac{q}{p}\right)_{B_d^0} = \frac{V_{tb}^* V_{td}}{V_{tb} V_{td}^*} = e^{2i\phi_M}. \tag{3.2}$$

The amplitudes for decays into a *CP* eigenstate f are

$$A \equiv \langle f|\mathcal{H}|B^0\rangle, \quad \overline{A} \equiv \langle f|\mathcal{H}|\overline{B}^0\rangle. \tag{3.3}$$

Let us define

$$r_{CP}(f) \equiv \frac{q}{p}\,\frac{\overline{A}}{A}. \tag{3.4}$$

The time-dependent rates for initially pure B^0 or $\overline{B}^0$ states to decay into a final *CP* eigenstate at time t can then be written as

$$\Gamma(B^0_{phys}(t) \to f) = |A|^2 e^{-\Gamma t} \times \left(\frac{1+|r_{CP}(f)|^2}{2} + \frac{1-|r_{CP}(f)|^2}{2}\cos(\Delta M t) - \mathrm{Im}\ r_{CP}(f)\ \sin(\Delta M t)\right), \tag{3.5}$$

$$\Gamma(\overline{B}^0_{\mathrm{phys}}(t) \to f) = |A|^2 e^{-\Gamma t} \times \left(\frac{1+|r_{CP}(f)|^2}{2} - \frac{1-|r_{CP}(f)|^2}{2}\cos(\Delta M t) + \mathrm{Im}\ r_{CP}(f)\ \sin(\Delta M t)\right). \tag{3.6}$$

The time-dependent *CP* asymmetry

$$a_f(t) = \frac{\Gamma(B^0(t) \to f) - \Gamma(\overline{B}^0(t) \to f)}{\Gamma(B^0(t) \to f) + \Gamma(\overline{B}^0(t) \to f)} \tag{3.7}$$

is given by

$$a_f(t) = \frac{(1-|r_{CP}(f)|^2)\ \cos(\Delta M t) - 2\,\mathrm{Im}\ r_{CP}(f)\ \sin(\Delta M t)}{1+|r_{CP}(f)|^2}. \tag{3.8}$$

This result holds for a *CP*-even final state, while for *CP*-odd states there is an additional minus sign in $r_{CP}(f)$. When only a single amplitude with a given weak decay phase ϕ_D dominates the decay, one has

$$\frac{\overline{A}}{A} = e^{-2i\phi_D}. \tag{3.9}$$

Since $\mathrm{Im}\ r_{CP}(f) = \sin 2(\phi_M - \phi_D)$, Equation 3.8 simplifies to

$$a_f(t) = -\sin 2(\phi_M - \phi_D)\sin(\Delta M t). \tag{3.10}$$

In an e^+e^- B Factory, the initial B^0 and $\overline{B}^0$ are produced in a coherent $B^0\overline{B}^0$ state and remain in this state until one of the particles decays. If one B decays to a flavor-tagging mode and the other decays to a *CP*-study mode, the event can be used to reconstruct the time dependence of the asymmetry. In this case, the time t in the equations above is the time between the tagging decay and the *CP*-study-mode decay. The tagging decay may be the later decay, in which case $t < 0$. Thus, the time-integrated *CP* asymmetry vanishes if $|r_{CP}(f)| = 1$, which makes essential a measurement of the time dependence. The asymmetric machine configuration and an accurate vertex determination make this possible.

The Standard Model predictions for *CP* violation are most often presented in terms of the unitarity constraints for the three-generation CKM matrix. If one assumes the Standard

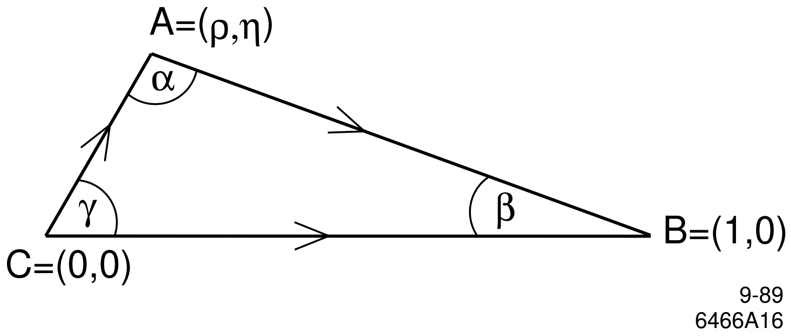

Figure 3-1. *The Unitarity Triangle.*

Model, one can derive relationships between the mixing phases and the weak phases of various contributions to the decay amplitudes and the angles of a triangle, generally called the Unitarity Triangle. Unitarity of the CKM matrix requires, among others, the relationship

$$V_{tb}V_{td}^* + V_{cb}V_{cd}^* + V_{ub}V_{ud}^* = 0. \tag{3.11}$$

The three complex quantities $V_{id}V_{ib}^*$ can be represented as a triangle in the complex plane. The three angles of this triangle are labeled

$$\alpha \equiv \arg\left(-\frac{V_{td}V_{tb}^*}{V_{ud}V_{ub}^*}\right), \tag{3.12}$$

$$\beta \equiv \arg\left(-\frac{V_{cd}V_{cb}^*}{V_{td}V_{tb}^*}\right), \tag{3.13}$$

$$\gamma \equiv \arg\left(-\frac{V_{ud}V_{ub}^*}{V_{cd}V_{cb}^*}\right). \tag{3.14}$$

Figure 3-1 shows the unitarity triangle, as it is usually drawn, rescaled by the side $V_{cd}V_{cb}^*$. This makes the base of the triangle real and of unit length. The apex of the triangle is then the point (ρ, η) in the complex plane, in the notation introduced by Wolfenstein [Wol85] for the parameters of the CKM matrix.

To overdetermine the unitarity triangle, experiments must fix as many of the parameters as possible that give the sides, $|V_{tb}V_{td}^*|/|V_{cb}V_{cd}^*|$ and $|V_{ub}V_{ud}^*|/|V_{cb}V_{cd}^*|$, and the angles, α, β, and γ. Defining $\lambda = V_{us} = \sin\theta_{Cabibbo}$, the quantities $V_{td} = \lambda$, $V_{ud} = \cos\theta_{Cabibbo}$, and $V_{tb} = 1$ are already well-determined up to terms of $O(\lambda^4)$. The value of V_{cb} will be well-determined by the study of semileptonic B decays at CLEO II, with possible further improvement from BaBar. Thus, the primary aim of the B Factory must be to measure accurately the magnitudes of V_{ub}, V_{td}, and the CP-violating asymmetries in the decay modes $B_d \to J/\psi K_S^0$, $B_d \to J/\psi K_L^0$, $B_d \to J/\psi K^*$, $B_d \to D^+D^-$, $B_d \to D^{*+}D^{*-}$, and $B_d \to \pi^+\pi^-$, $B_d \to \rho\pi$. Determination

Quark Process	B_d Mode	$\phi_M - \phi_D$
$b \to c\overline{c}s$	$J/\psi\, K^0_S$ $J/\psi\, K^0_L$ $J/\psi\, K^{0*}$	β
$b \to c\overline{c}d$	D^+D^- $D^{+*}D^{-*}$ $D^{\pm *}D^{\mp}$	β
$b \to u\overline{u}d, d\overline{d}d$	$\pi^+\pi^-$ $\rho^{\pm}\pi^{\mp}$ $a_1^{\pm}\pi^{\mp}$	α

Table 3-1. *CP modes and Standard Model asymmetry predictions for B_d decays.*

of CKM elements will be discussed below. First, we concentrate on the time-dependent *CP* asymmetries.

Table 3-1 shows the Standard Model relationship between the angles of the unitarity triangle and the predicted $arg(r_{CP}(f)) = 2(\phi_M - \phi_D)$, assuming a single weak decay amplitude dominates in each of these cases. In addition to pure *CP* eigenstates, other channels with *CP*-self-conjugate quark content can be analyzed for *CP*-violating contributions. These include mixed spin states such as $J/\psi\, K^*$ and vector-scalar mixtures such as $\rho\pi$ and D^*D where the various possible charge assignments have both *CP* and isospin relationships [Ale91, Ale93].

For the $b \to c\overline{c}s$ decays, which give channels that measure the angle β, we are in a fortunate situation. Up to corrections of order $A\lambda^4$, the penguin diagrams have the same weak phase as the tree diagrams. Thus, these channels have an unambiguous relationship between the measured asymmetry and the angle β. For channels that measure the angle α, the situation is not quite as good, although still satisfactory. In this case, QCD penguin diagrams are expected to give contributions on the order of perhaps 5–20% of the tree amplitude, and they have a different weak phase. In addition, the Z^0-mediated penguin diagram also contributes at the level of perhaps 5% of the tree amplitude, with the same weak phase as the QCD penguins [Des95]. Isospin-based analysis can select an isospin channel that has no QCD-penguin contribution [Gro90]. The uncertainty in $\sin 2\alpha$ extracted from the asymmetry in this channel due to the Z^0-penguin contributions is then not more than 0.05%. This is less than the expected experimental uncertainty. Furthermore, an isospin-based analysis will give a measure of the total penguin contributions, and hence, can be used to tighten the bounds on the possible Z^0-penguin effects. In addition, measurement of the time dependence of the asymmetry will allow us to fit the $\cos(\Delta M t)$ behavior as well as the $\sin(\Delta M t)$ in Equation 3.8. This then gives a further constraint on the magnitude of penguin contributions.

Isospin analyses can probably be carried out most effectively for the $\rho\pi$ channels, since all three channels decay to $\pi^+\pi^-\pi^0$ and so have similar detection efficiencies. This channel has the additional advantage that the interference regions between the different charge combinations of $\rho\pi$ give further information, allowing a determination of $\sin 2\alpha$ and $\cos 2\alpha$ which resolves the ambiguity between α and $90 - \alpha$ [Qui93]. For the $\pi\pi$ case, the isospin analysis requires a measurement of the rates for $B^0 \to \pi^0\pi^0$ and $B^+ \to \pi^+\pi^0$.

The simulation estimates for the accuracy of α measurements given below, assume that penguin contributions are sufficiently small that the measured asymmetries can be used directly to determine α without isospin analysis. The isospin analysis can be used to check this assumption and to obtain a penguin-corrected value. The degradation in accuracy due to this multichannel analysis is not expected to be large.

3.2 Simulation Tools

Detailed simulation work has been performed to determine the efficiency of the proposed detector to make the necessary measurements of the channels of interest and to ascertain that backgrounds can be simultaneously reduced to an acceptable level. Studies of tagging modes have also been carried out. Two different Monte Carlo simulation packages, ASLUND and BBSIM, were used for this purpose. ASLUND is a fast parametric Monte Carlo, while BBSIM is a detailed simulation based on the GEANT package [CER93]. Both are designed to be flexible, so that variations in detector design can be investigated. Brief descriptions of each are given below. Where not otherwise noted, branching ratio information is taken from the 1994 PDG compilation [PDG94].

3.2.1 ASLUND

ASLUND consists of two major components: the JETSET 7.3 [Sjo93] event generator configured for the PEP-II environment and a parametric simulation of the detector. Other generators (*e.g.,* KORALB [Jad90]) are available using the interface routine BEGET [Wri94]. The parametric simulation includes charged tracking, particle identification, and calorimetry.

Charged particle tracking is simulated using the TRACKERR package [Inn93] to estimate the fully correlated error matrix, which is then used to smear the track parameters. The main drift chamber, the silicon vertex detector, and any intervening material are modeled. The TRACKERR input format is used to specify detector geometry, measurement precision, and material distribution. The combination of ASLUND and TRACKERR has been compared to BBSIM for the mode $B^0 \to \pi^+\pi^-$ and found to agree within 15% for the predicted B^0 mass width.

Subdetector	Simulation Level
Beam Line, Beam Pipe, and Support Tube	Geometry
Silicon Vertex Detector	Digitizations
Drift Chamber	Hits
DIRC	Digitizations
ATC	Geometry
CsI Calorimeter	Hits
Coil and Instrumented Flux Return	Digitizations

Table 3-2. *BaBar subdetectors modeled in BBSIM.*

Simulation of particle identification ($\pi/K/p$) information is available for dE/dx, DIRC, and aerogel threshold counters (ATCs). The geometrical configuration of these devices can also be specified using the TRACKERR format, and performance parameters can be varied to assess the sensitivity to detector capabilities.

The geometry of the calorimeter, and any material in front of it can also be specified in the TRACKERR format. Photons converted into e^+e^- pairs in the material in front of the calorimeter are tracked to determine whether or not they will deposit any energy in the calorimeter. Energy loss in material and acceptance losses due to the curl-up in the magnetic field are taken into account in determining the calorimeter signal. A detailed parameterization of the calorimeter response based on GEANT simulations has been developed for some analyses, *e.g.,* $\rho\pi$ and DD. Analogous to the other devices discussed above, energy and angular resolutions can be varied by modifying simple parameters.

3.2.2 GEANT Simulation—BBSIM

Simulation packages for event generation (BEGET), detector response, and subsequent analysis (BBSIM) have been written to aid in the design and optimization of the *BaBar* detector.

The generation of an event from an e^+e^- collision and the subsequent loading of decay products into GEANT banks is handled by the BEGET [Wri94] package. The generators currently available include $\Upsilon(4S)$ decays and hadronic continuum events via JETSET [Sjo93] and $\tau^+\tau^-$ decays via KORALB [Jad90]. BEGET is capable of overlaying background hits originating from beam-gas collisions on simulated events.

The BBSIM package is based on the CERN detector description and simulation tool, GEANT [CER93]. The latter consists of packages to construct the detector geometry using a set of 15 different volume types; to step charged and neutral particles through the detector,

Cut	$\pi^+\pi^-$	$\pi^0\pi^0$
Geometry and Lepton ID Inefficiency	0.82	0.82
J/ψ Invariant Mass From 0.14 to 0.44 MeV/c	1.00	1.00
Combined J/ψ Efficiency	0.82	0.82
Geometry, Efficiency and Track/Photon Cuts	0.78	0.55
π^0 Association Cuts	-	0.89
π^0 Mass Cuts	-	0.93
K^0_s Momentum $0.9 \leq$ p ≤ 2.9 MeV/c	-	1.00
K^0_s Invariant Mass	0.94	1.00
Combined K^0_s Efficiency	0.73	0.45
B^0 Momentum From 0.14 to 0.44 MeV/c	0.99	0.99
B^0 Candidate Mass	1.00	0.96
Overall B^0 Reconstruction Efficiency	0.59	0.35

Table 3-3. *Summary of efficiencies for B^0 reconstruction in $B^0 \to J/\psi K^0_S$.*

simulating the full variety of interactions with the detector; to define, register, and digitize the Monte Carlo track hits (typically track positions and directions); and to display the detector components, particle trajectories, and track hits. The BBSIM framework consists of a driver routine to invoke GEANT; a database facility, DBIN, to define detector geometry, materials and media; and a set of subpackages, one per detector subsystem, to define the subdetector geometry, register track hits, simulate the detector response, store the results, and perform subsequent analysis. The subsystems included in BBSIM, and the corresponding levels of simulation, are shown in Table 3-2.

3.3 Studies of $B^0 \to J/\psi$ Modes

3.3.1 $B^0 \to J/\psi K^0_S$

The analysis of this channel and a study of the background were performed using the ASLUND Monte Carlo. This work is described in more detail in Reference [Har95]. The results are based on an assumed branching ratio of 0.5×10^{-3}, calculated using isospin from the measured $B^+ \to J/\psi K^+$ rate [PDG94].

The efficiencies obtained are summarized in Table 3-3. The analysis proceeded as follows.

- Candidate $J/\psi \to \ell^+\ell^-$ events were selected. Lepton identification efficiencies (calculated using BBSIM) and a J/ψ mass cut were applied, and K^0_Ss were reconstructed in both the charged and neutral decay modes. In the charged mode, the invariant mass was required to be within $\pm 25\,\mathrm{MeV}/c^2$ of the nominal K^0_S mass. To help suppress the combinatorial background in the neutral mode, various cuts were made on the consistency of the four photons having a common point of origin while also being consistent with the two π^0 sub-masses, and the K^0_S mass and lifetime. The invariant mass was required to be within $\pm 40\,\mathrm{MeV}/c^2$ of the nominal K^0_S mass. Note that reconstruction of the neutral K^0_S decays requires the calorimeter to reconstruct the π^0s.

- Candidate J/ψ and K^0_S events were combined to form B^0 candidates. A cut was applied on the B^0 momentum in the $\Upsilon(4S)$ rest frame (kinematically, this is $\sim 340\,\mathrm{MeV}/c$). The invariant mass of the B^0 candidate was required to be between 5.20 and $5.36\,\mathrm{GeV}/c^2$.

Potential backgrounds to this decay mode include those from $B^0 \rightarrow J/\psi X$, cascade semi-leptonic decays ($b \rightarrow cl^- \overline{\nu} \rightarrow sl^+ l^- \nu\overline{\nu}$), and continuum production of quark-antiquark pairs. Large numbers of each were generated and passed through the analysis described above. The fractions of events surviving all the cuts are summarized in Table 3-4. Also shown are the relative production rates compared to signal events, given by

$$\text{normalization} = \frac{\sigma_{BG} \times B(BG)}{\sigma_{b\bar{b}} \times B(B^0 \rightarrow \text{channel})}.$$

The predicted upper limit on the number of background events per reconstructed signal B^0 is given for each source. No background events survived the cuts in these simulations. All backgrounds together contribute no more than 6%. These levels are considered negligible for the extraction of $\sin 2\beta$ from the decay asymmetry.

3.3.2 $B^0 \rightarrow J/\psi K^0_L$

The branching ratio for this channel is the same as that for $J/\psi K^0_S$, but the expected asymmetry has the opposite sign. Thus, high-efficiency detection of K^0_Ls can provide an alternate measurement of β and improve the overall accuracy with which this parameter is determined.

A study of the mode $B^0 \rightarrow J/\psi K^0_L$ has been carried out [Wri94b]. Since the K^0_L momentum is not well-measured, the K^0_L direction and the J/ψ momentum are combined, and a B-mass constraint is applied to determine p_{rest}, the momentum of the B in the $\Upsilon(4S)$ rest frame. The resulting distribution for p_{rest} is shown in Figure 3-2, in which only events from the $\Upsilon(4S)$ are shown; continuum backgrounds in this channel are negligible, as with other J/ψ channels. A cut $p_{rest} \leq 0.42\,\mathrm{GeV}/c$ is made to eliminate false combinations.

Channel	Efficiency	Normalization	# per observed signal event
Charged Mode search:			
$J/\psi K^0_S \to l^+l^-\pi^+\pi^-$	0.59	1.00	1.00
$J/\psi X$	7×10^{-4}	3.9×10^{1}	4.6×10^{-2}
Semileptonic	8×10^{-7}	7.8×10^{2}	1×10^{-3}
$q\overline{q}$ continuum	1.3×10^{-7}	8.1×10^{4}	1.8×10^{-2}
Neutral Mode search:			
$J/\psi K^0_S \to l^+l^-\pi^0\pi^0$	0.35	1.00	1.00
$J/\psi X$	5×10^{-5}	7.8×10^{1}	1.1×10^{-2}
Semileptonic	1×10^{-7}	1.6×10^{3}	4.7×10^{-4}
$q\overline{q}$ continuum	1×10^{-7}	1.6×10^{5}	4.7×10^{-2}

Table 3-4. *Background contributions for the $J/\psi K^0_S$ channel.*

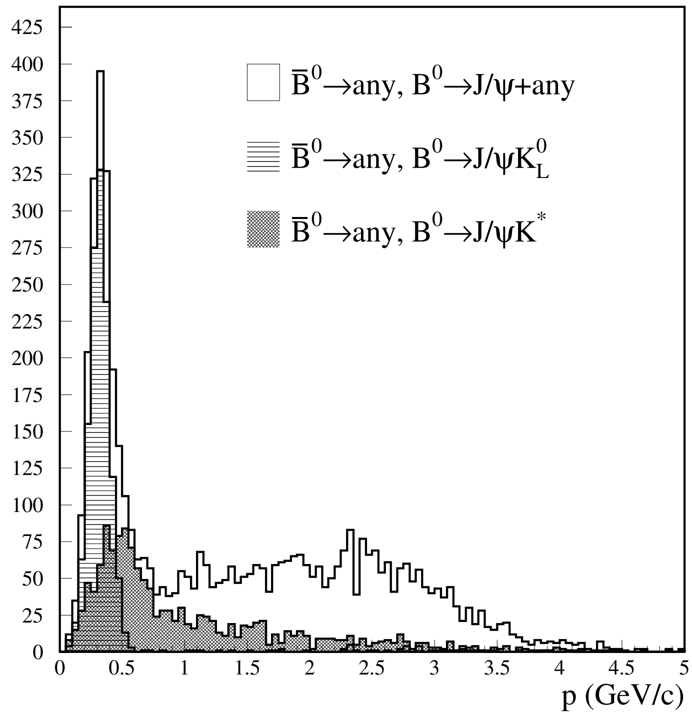

Figure 3-2. *Momentum distribution of B^0 (p_{rest}) from $\Upsilon(4S) \to B\bar{B}$ in the $\Upsilon(4S)$ rest frame, including the effect of the nominal e^+e^- beam smearing and K^0_L angular resolution.*

Sample	Reconstruction Efficiency	# Reconstructed	Background From K^*	Other Background
Low K^*	0.25	544	31	74
High K^*	0.08	168	65	117
Combined	0.33	712	96	191

Table 3-5. *Efficiencies for B^0 reconstruction and sensitivity to α for $B^0 \to J/\psi\, K^0_L$.*

One sees that a substantial background which survives this cut comes from $B^0 \to J/\psi\, K^*$ with $K^* \to K^0_L \pi^0$. Since the asymmetry for $J/\psi\, K^*$ is opposite in sign to that for $J/\psi\, K^0_L$, these events contribute to a dilution of the measured asymmetry in the same fashion as do wrong-sign tags. In order to obtain an accurate estimate of the error on the asymmetry, the data is divided into two samples, one with a low K^* background and the other with a higher background. The two samples are then treated independently in determining β sensitivity. The high K^* background sample is defined as follows: any pion in the event is combined with the K^0_L to define K^* candidates. The K^0_L momentum is recalculated under this assumption along with a B mass constraint. Any event in which a candidate K^* has a mass within $\pm 30\,\mathrm{MeV}/c^2$ of the true K^* mass is assigned to the high background sample. Events with no K^* candidates are assigned to the low background sample. Table 3-5 shows the results for the separate samples and the combined sensitivity for this channel.

3.3.3 $B^0 \to J/\psi\, K^{0*}$

Only the neutral decay mode of the K^{0*} is useful for *CP*-violation measurements. The analysis of this channel and a study of the background were performed using the ASLUND Monte Carlo and the published $B^0 \to J/\psi\, K^{0*}$ branching ratio of 1.6×10^{-3} [PDG94]. The analysis proceeded in a manner similar to that for $B \to J/\psi\, K^0_S$ described above. First, J/ψ and K^0_S candidates were formed as above, where only the charged decay mode of the K^0_S was used in this case. Candidate π^0s were obtained from pairs of calorimeter clusters, assuming that the photons originated at the nominal interaction position of the experiment. All combinations of π^0 and K^0_S candidates were made, and a mass cut applied to the resulting K^{0*} candidates. All mass cuts and the various subefficiencies of each stage of the reconstruction are summarized in Table 3-6.

Cut	Efficiency
Geometry and Lepton ID Inefficiency	0.82
$3.06 < J/\psi$ Mass < 3.14 GeV/c^2	1.00
Combined J/ψ Efficiency	0.82
Geometry and $E_{\gamma min} = 25$ MeV/c^2	0.73
$0.120 < \pi^0$ Mass < 0.150 GeV/c^2	0.95
Combined π^0 Efficiency	0.69
Geometry and Track Cuts	0.77
$0.468 < K^0_S$ Mass < 0.528 GeV/c^2	0.92
Combined K^0_S Efficiency	0.71
Combined K^{0*} Sub-efficiencies	0.50
$0.73 < K^{0*}$ Mass < 1.05 GeV/c^2	0.98
Overall K^{0*} Efficiency	0.50
Combined B^0 Sub-efficiencies	0.40
B^0 Momentum in Υ Rest Frame	0.99
B^0 Candidate Mass	0.99
Overall B^0 Reconstruction Efficiency	0.39

Table 3-6. *Cuts and Efficiencies for B^0 Reconstruction in $B^0 \to J/\psi K^{0*}$.*

3.4 Studies of B^0 to Double Charm Modes

3.4.1 $B^0 \to D^+D^-$

A branching fraction of 6×10^{-4} is used for this channel and is obtained by averaging the measured branching fractions for B^+ and B^0 to decay to DD_S and multiplying by $\sin^2\theta_C$.

Only those D^+ modes with no more than one π^0 and a branching fraction greater than about 1% are considered. Only those K^0_Ss in the $\pi^+\pi^-$ decay mode are included. The channels used are shown in Table 3-7 with branching ratios taken from Reference [PDG94]. The mass resolutions quoted are vertex constrained. The efficiency for each mode in Table 3-7 includes cuts on particle identification for each track and a cut on χ^2 probability for the reconstructed D vertices at 2%. Mass cuts of $\pm 3\sigma_{m_D}$ are made on each D meson candidate.

Pairs of D meson candidates are combined to form B candidates. Each B candidate is required to have a total momentum between 180 and 440 MeV/c in the $\Upsilon(4S)$ rest frame. A vertex and kinematic fitting package is then used to fit the entire B event, constraining the intermediate D masses and vertices and the two Ds to a single vertex. The χ^2 probability

Mode	Branching Fraction	Single D Efficiency	σ_{m_D}(MeV)
$K^-\pi^+\pi^+$	0.091	0.67	4.3
$K^-\pi^+\pi^+\pi^0$	0.064	0.42	6.9
$K^0_S\pi^+$	0.014	0.59	5.0
$K^0_S\pi^+\pi^0$	0.049	0.38	9.1
$K^0_S\pi^-\pi^+\pi^+$	0.035	0.41	3.7
$K^0_S\pi^-\pi^+\pi^+\pi^0$	0.027	0.26	5.5

Table 3-7. *Efficiency and mass resolutions for D^+ reconstruction.*

$B \to D^+D^- \to$	Branching Fraction ($\times 10^{-3}$)	Efficiency	σ_{m_B} (MeV)	σ_{z_B} (μm)	# of Events in 30 fb^{-1}	S/B
$D^+ \to K^-\pi^+\pi^+$ $D^- \to K^+\pi^-\pi^-$	8.3	0.45	5.0	47.0	80.0	1.8
$D^+ \to K^-\pi^+\pi^+$ $D^- \to K^+\pi^-\pi^-\pi^0$	11.6	0.24	6.5	54.0	61.0	0.7
$D^+ \to K^0_S\pi^+$ $D^- \to K^+\pi^-\pi^-$	2.5	0.38	5.3	58.0	14.0	> 3.0

Table 3-8. *Efficiency, mass and vertex resolution, signal, and background for three of the D decay mode combinations used in the $B \to D^+D^-$ reconstruction.*

for this fit is required to be greater than 2%. The reconstructed mass is required to lie within $\pm 20\,\text{MeV}/c^2$ of the B^0 mass. For events passing the above cuts, a B mass constraint is added to determine the B decay point. There are many combinations of the D decay modes listed in Table 3-7, each with different efficiencies and resolutions. Table 3-8 gives the efficiencies and resolutions for three of the 21 combinations. The complete set of numbers can be found in Reference [Cou95].

Potential sources of background are from other decays of the $\Upsilon(4S)$ and continuum quark-antiquark production. Table 3-8 includes an estimate of signal-to-background ratios (S/B) for the modes discussed. Channels with two or more π^0s in the final state tended to have large backgrounds and were, therefore, not included in this analysis. Although each combination of D decay modes is analyzed separately, one can sum over all modes to obtain a total reconstructable branching fraction of 0.044, an average acceptance of 0.27, and a final event sample of 259 events with a background of 351 events.

Mode	Branching Fraction	Single D^0 Efficiency	$\sigma_{m_{D^0}}$ (MeV)
$K^-\pi^+$	0.040	0.77	5.2
$K^-\pi^+\pi^0$	0.138	0.48	8.8
$K^0_S\pi^+\pi^-$	0.026	0.48	4.0
$K^0_S\pi^+\pi^-\pi^0$	0.049	0.29	6.8
$K^-\pi^+\pi^+\pi^-$	0.081	0.55	3.7
$K^-\pi^+\pi^+\pi^-\pi^0$	0.043	0.34	5.5

Table 3-9. *Efficiency for reconstruction of D^0s produced in $B \to D^{*+}D^{*-}$ decays.*

3.4.2 $B^0 \to D^{*+}D^{*-}$

A branching fraction of 1.5×10^{-3} is used for this mode which is 2.5 times larger than that for D^+D^-. This factor is the typical increase for vector-vector decay modes over comparable scalar-scalar channels.

The only decay chain considered is that in which each $D^{*\pm}$ decays to $D^0\pi^\pm$ with a branching fraction of $68 \pm 1.6\%$. The efficiency for finding the slow pions has been studied in more detailed simulations of the vertex detector and found to be better than 95% over the momentum range of interest above $p_t = 60\,\mathrm{MeV}/c$ for $\theta > 300\,\mathrm{mr}$. The branching fraction, efficiency, and mass resolution for the D^0 modes are given in Table 3-9.

In reconstructing D^* mesons, all D^0 candidates are combined with charged pions and a cut made at $\pm 3\sigma$ on the D^*–D^0 mass difference. Pairs of D^* candidates are then fit for the B mass, constraining the vertex and mass of the intermediate D^* and D^0. Table 3-10 gives the efficiency, resolutions, and background levels for three of the 21 combinations. The complete set of results can be found in Reference [Cou95]. Although each combination of D^0 decay modes is analyzed separately, one can sum over the modes to obtain a total reconstructable branching fraction of 0.125, an average acceptance of 0.15, and a final event sample of 473 events with a background of 21 events.

In computing *CP* reach, $D^{*+}D^{*-}$ channels are assumed to be dominated by a single *CP* state. If this turns out not to be the case, a partial-wave analysis will need to be performed to disentangle the *CP* = + and *CP* = − states. This will decrease the effectiveness of these channels by a factor that depends on the fraction of each *CP* state present.

$B \to D^{*+}D^{*-} \to$	Branching Fraction ($\times 10^{-3}$)	Efficiency	σ_{m_B} (MeV)	σ_{z_B} (μm)	# of Events in 30 fb^{-1}	S/B
$D^0 \to K^-\pi^+$ $D^0 \to K^+\pi^-$	1.6	0.41	5.6	53.0.	16.0	> 2.0
$D^0 \to K^-\pi^+$ $D^0 \to K^+\pi^-\pi^0$	11.0	0.21	5.8	65.0	58.0	> 7.0
$D^0 \to K^0_S\pi^+\pi^-$ $D^0 \to K^+\pi^-$	2.1	0.29	4.3	55.0	10.0	> 1.2

Table 3-10. *Efficiency, mass and vertex resolution, signal, and background for three of the D decay mode combinations used in the $B \to D^{*+}D^{*-}$ reconstruction.*

3.4.3 $B \to DD^*$

While this mode is not a *CP* eigenstate, *CP*-violating asymmetries can be measured using both $D^{*+}D^-$ and $D^{*-}D^+$ data [Ale91]. A full simulation of these modes has not been carried out, but efficiencies and backgrounds can be estimated using the two previous studies. The decays $B \to D^{*-}D_s^+$ and $B \to D^-D_s^{*+}$ have been observed with branching ratios of $1.2\pm0.6\%$ and $2.1 \pm 1.5\%$, respectively [PDG94]. Rescaling by $\sin^2\theta_C$ gives reasonable estimates for the DD^* rates. Using the acceptances determined in the two previous sections we predict a total reconstructable branching fraction of 0.085, an average acceptance of 0.168, and a final event sample of 557 events.

3.5 Studies of $B \to \pi\pi$ Modes

The measurement of $\sin 2\alpha$ from a *CP*-violating asymmetry in the $B^0 \to \pi^+\pi^-$ mode requires the selection of rather clean samples of $\pi^+\pi^-$ as well as $\pi^\pm\pi^0$ and $\pi^0\pi^0$ events [Ale92]. The latter are needed for an isospin analysis to estimate the size of the penguin contribution to the total decay amplitude and to extract $\sin 2\alpha$ from the *CP* asymmetry for the case in which the QCD-penguin amplitudes are large [Gro90]. Unfortunately, the branching ratios for charmless two-body B decays into either pions or kaons are expected to be very small, on the order of 10^{-5} or less [Bro93]. Therefore, these channels suffer from a potentially large background due to continuum quark-antiquark pair production, despite a clean signature. Simple cuts strongly reduce the continuum background and allow one to enrich the sample in two-body B^0 decays. In addition, the branching ratio of $B \to K\pi$ modes may be comparable to $B \to \pi\pi$. In order to disentangle the $\pi^+\pi^-$ component of the signal from $K^\pm\pi^\mp$ events, a very good particle identification system operating up to high momentum (4–4.5 GeV/c) is needed. This is one of the main features of the BABAR detector. Studies for all of these channels have been performed using both ASLUND and BBSIM. Because of the large sample of Monte-Carlo events needed, the continuum background was studied using ASLUND only. The branching ratio for $B \to \pi^+\pi^-$ is taken to be 1.2×10^{-5}, which is based on the measurement from CLEO [Bat93a].

3.5.1 $B^0 \to \pi^+\pi^-$

Despite apparent simplicity, analysis of this mode, dealing with rejection factors at the 10^{-5} to 10^{-6} level, requires a precise knowledge of detector systematics. Strong track quality cuts will be needed; these are not included in the present study. Software tools (full detector simulation and pattern recognition packages) are being developed and will be used to refine the selection cuts and to give more accurate estimates of signal efficiencies and background rejection.

Reduction of Continuum Background

The reduction of the continuum background is achieved by cuts applied in the $\Upsilon(4S)$ center-of-mass frame. The first two cuts exploit the fact that the B mesons are produced almost at rest, and thus the pions are almost monoenergetic, in the $\Upsilon(4S)$ rest frame. The third uses the fact that continuum background events are mostly jet-like, whereas $B^0\overline{B}^0$ decays are not. A cut on particle identification ($\Delta\chi^2$) gives a significant background reduction. This occurs because the sample of background tracks hard enough to masquerade as a $B \to \pi\pi$ event is enriched in kaons and protons.

Charged particles of momentum $p^\star$ in the $\Upsilon(4S)$ center of mass are selected in a very narrow range: $2.35 \le p^\star(\pi^\pm) \le 2.95\,\mathrm{GeV}/c$. This momentum window contains virtually 100% of reconstructed pions (or kaons) from two-body decays. The probability that a continuum charged particle lies in this momentum window is less than 2%. The probability that a continuum event contains two such particles with opposite electric charge is 3.3×10^{-3}.

Any selected pair of opposite sign particles forms a B^0 candidate. The B^0 candidate momentum $p^\star(B)$ in the $\Upsilon(4S)$ center of mass frame is required to lie in the 150–500 MeV/c range. This cut selects pairs with large opening angles. To be conservative, we have used a rather large window for the B^0 mass cut. The signal-to-background ratio (S/N) is a strong function of the angle θ_{sph} between the B-decay axis and the sphericity axis formed by the remaining tracks in the event. The background is strongly peaked at $cos\theta_{sph} = \pm 1$ while the distribution of the signal in this variable is flat. We divide the data into 3 bins (< 0.7, 0.7–0.9, and 0.9–1.0) in $|cos\theta_{sph}|$ in order to optimize the CP-sensitivity in this channel. The

Cut	$B^0 \to \pi^+\pi^-$	$q\overline{q}$
$\pi^+\pi^-$ Acceptance and $p^\star(\pi^\pm)$ in $[2.35, 2.95]$	0.862	3.3×10^{-3}
0 : Preselected Events (Normalization)	1.000	1.000
1 : $p^\star(B)$ in $[0.150, 0.500]$	0.994	0.246
2 : $\Delta\chi^2 \geq 0$	0.972	0.275
$1+2+\lvert cos\theta_{sph}\rvert < 0.7$	0.538	5.0×10^{-6}
$1+2+0.7 < \lvert cos\theta_{sph}\rvert < 0.9$	0.166	6.0×10^{-6}
$1+2+0.9 < \lvert cos\theta_{sph}\rvert < 1.0$	0.094	3.9×10^{-5}
Overall Efficiency per Event Generated	0.798	5.0×10^{-6}

Table 3-11. *Efficiencies of background rejection cuts for the $B^0 \to \pi^+\pi^-$ mode.*

particle identification requirement on $\Delta\chi^2$ is explained in the following section. The results are summarized in Table 3-11.

Particle Identification

The rejection of $K\pi$ events from the sample is a crucial step in measuring the correct asymmetry. The criterion used combines information from kinematics (mass resolution), dE/dx, and the DIRC particle identification system. The quality of all three pieces of information is essential to obtaining good background rejection without significant loss of signal.

Combining all kinematic and PID information leads to a χ^2 test with up to five degrees of freedom. In reality, within the acceptance of *BaBar*, one particle lies outside of the DIRC acceptance ~10% of the time. Thus, the number of measurable degrees of freedom differs from event to event. We define a discriminating variable $\Delta{\chi_i}^2$ as the average χ^2 difference between the null hypothesis ($\pi\pi$) and any one of the alternate hypotheses. The five possible terms are a kinematic term for the pair, $\Delta{\chi^2}_{kin}$, and two possible particle identification terms for each member of the pair, $\Delta\chi^2_{j\,dE/dx}$ and $\Delta\chi^2_{j\,DIRC}$. We retain only the hypothesis giving $\chi^2 \geq 0$. Simulation samples of $B^0 \to \pi\pi$ and $B^0 \to K\pi$ are used to determine α, the probability of rejecting a true $\pi\pi$ event, and β, the probability of accepting an event with a K, as functions of the minimum $\Delta\chi^2$ needed to reject the alternate hypotheses. The results obtained with ASLUND are listed in Table 3-12. One can see from this table that for a significance $\alpha = 5\%$, obtained for $\Delta\chi^2_{crit} \simeq 4$, β can be maintained below 1%. The simulation's results for the dE/dx and momentum resolutions are based on ideal performance of the drift chamber and are probably optimistic. They do not include the single cell efficiencies, track overlaps, background rate effects, polar angle dependence of the dE/dx response, or a myriad of other factors which need to be addressed by an operating

min $\Delta\chi^2$	0	4	9	0	4	9
	$1-\alpha$			β		
Kinematics	86	51	12	9.7	1.8	—
dE/dx	75	36	6	12	1.5	—
Kin. + dE/dx	92	80	53	4.7	1.1	—
DIRC	74	69	58	1.8	—	—
Kin. + dE/dx + DIRC	98	95	87	2.4	0.8	—

Table 3-12. *Probabilities for selecting a $\pi^+\pi^-$ event $(1-\alpha)$ and a $K^+\pi^-$ event (β), for several minimum values $\Delta\chi^2$, based on an ASLUND simulation.*

experiment. We note that neither CLEO nor ARGUS have been able to achieve reliable K/π separation for high momentum tracks with this method.

Results

The $\pi^+\pi^-$ events are separated into three classes for analysis of *CP* sensitivity [Sny95]. Class 1 contains events with $\cos\theta_{sph} < 0.7$, class 2 contains those with $0.7 \le \cos\theta_{sph} \le 0.9$, and class 3 is all other events. Using the results listed in Table 3-11 and assuming a branching ratio of 1.2×10^{-5} [Bat93a], one can reach a background to signal ratio (B/S) of around 2 with a large efficiency $\epsilon = 54\%$. While the backgrounds in classes 2 and 3 are higher, inclusion of these events still improves the overall sensitivity.

The effect of the difference between the signal and the background in Δz the axial separation of the two B decays, further reduces the impact of continuum backgrounds. This is discussed below.

3.5.2 $B^0 \to \pi^0\pi^0$

The reconstruction of π^0s from calorimeter data is discussed in Chapter 7. The resolution obtained on the π^0 mass using BBSIM is $8.3\,\mathrm{MeV}/c^2$. This leads to an efficiency of 84% for π^0 reconstruction, restricting π^0 candidates to the $[100-170\,\mathrm{MeV}/c^2]$ $\gamma\gamma$ mass window. The same mass window is chosen for background studies with ASLUND.

The results obtained with ASLUND for this mode are summarized in Table 3-13. We assume a branching ratio for $B \to \pi^0\pi^0$ of 5×10^{-6}. After selection of the $\pi^0\pi^0$ pair, the same kinematic cuts as in the $\pi^+\pi^-$ modes are applied. Using BBSIM, the resolution on the reconstructed B^0 mass in $\pi^0\pi^0$ is found to be $49.7\,\mathrm{MeV}/c^2$, dominated by the errors on the

Cut	$B^0 \to \pi^0\pi^0$	$q\overline{q}$
$\pi^0\pi^0$ Acceptance and $p^\star(\pi^0)$ in $[2.350, 2.950]$	0.849 (0.772)	0.6 $\times 10^{-3}$
0 : Preselected Events (Normalization)	1.000	1.000
1 : $p^\star(B)$ in $[0.150, 0.500]$	0.989	0.263
2 : Cosine Angle w.r.t. Sphericity Axis ≤ 0.8	0.770	0.115
3 : Cosine Angle w.r.t. Sphericity Axis ≤ 0.7	0.661	0.071
$1+2$	0.765	0.032
$1+2+m(\pi\pi)$ in $[5.120, 5.440]$	0.754	0.015
$1+3$	0.656	0.019
$1+3+m(\pi\pi)$ in $[5.120, 5.440]$	0.648	6.5 $\times 10^{-3}$
Overall Efficiency per Event Generated	0.550 (0.518)	4.0 $\times 10^{-6}$

Table 3-13. *Efficiencies of background rejection cuts for the $B^0 \to \pi^0\pi^0$ mode. The numbers quoted in parentheses are obtained when combinatorial background in signal events is suppressed.*

measurement of photon energies. The cut on the π^0 masses, together with a 3σ cut on the B^0 mass ($5.120 < m < 5.440\,\mathrm{GeV}/c^2$), yields an efficiency of 55% with a B/S of less than 4 to 1. These simulations have been made using a somewhat different detector geometry than given in this *Technical Design Report*, but the conclusions are still valid.

3.5.3 $B^+ \to \pi^+\pi^0$ Decays

In addition to the $\pi^0\pi^0$ mode, the isospin analysis requires results from $B^+ \to \pi^+\pi^0$ decays. A treatment similar to that described above has been made for this mode, and the results are presented in Table 3-14. An efficiency of 53% is achieved with a B/S of less than 3.5 to 1 using an assumed branching ratio of 1.2×10^{-5}.

3.6 $B^0 \to \rho^\pm\pi^\mp$

The branching ratio for $B^0 \to \rho^+\pi^-$ is taken to be $(f_\rho/f_\pi)^2 \times BR(B^0 \to \pi^+\pi^-) = 2.9 \times 10^{-5}$. The value $(f_\rho/f_\pi)^2 = 2.4$ is determined from $\tau \to \rho\nu$ and $\tau \to \pi\nu$ data [PDG94]. This number is higher than that used in the *Letter of Intent* because recent LEP data on $\tau \to \rho\nu$ has caused a significant increase in the best fit value. The corresponding rate for $B \to \pi^+\rho^-$ is more model dependent; we use $R = \Gamma(B^0 \to \pi^+\rho^-)/\Gamma(B^0 \to \rho^+\pi^-) = 1$. Estimates for

Cut	$B^+ \to \pi^+\pi^0$	$q\overline{q}$
$\pi^+\pi^0$ Acceptance and $p^\star(\pi)$ in $[2.35, 2.95]$	0.863 (0.803)	3.8 $\times 10^{-3}$
0 : Preselected Events (Normalization)	1.000	1.000
1 : $p^\star(B)$ in $[0.150, 0.500]$	0.987	0.252
2 : $\lvert$Cosine Angle w.r.t. Sphericity Axis$\rvert \leq 0.8$	0.756	0.120
3 : $\lvert$Cosine Angle w.r.t. Sphericity Axis$\rvert \leq 0.7$	0.650	0.069
4 : $\Delta\chi^2 \geq 0$	0.942	0.487
$1+2+4$	0.717	0.013
$1+2+4+m(\pi\pi)$ in $[5.150, 5.410]$	0.713	4.5 $\times 10^{-3}$
$1+3+4$	0.617	6.2 $\times 10^{-3}$
$1+3+4+m(\pi\pi)$ in $[5.150, 5.410]$	0.614	2.3 $\times 10^{-3}$
Overall Efficiency per Event Generated	0.529 (0.506)	8.5 $\times 10^{-6}$

Table 3-14. *Efficiencies of background rejection cuts for the $B^+ \to \pi^+\pi^0$ mode. The numbers quoted in parentheses are obtained when combinatorial background in signal events is suppressed.*

the ratio range from a high of 15 [Ale91] to a low of about 1/12 [Dea93]. The sensitivity of $\delta\alpha$ to this ratio varies as $\sqrt{(R+1)/2R}$.

An analysis of this channel and a study of the background were performed using the ASLUND Monte Carlo. The calorimeter performance was determined using BBSIM and was parameterized for the study. Only the backgrounds due to production of quark-antiquark pairs in the continuum have been considered, as they are expected to be the dominant source. Other $\rho\pi$ channels decay to the same final state, $\pi^+\pi^-\pi^0$, and will be subject to similar backgrounds. Eventually, all three possible final states will need to be studied to allow a full isospin analysis. However, it is sufficient to show that the detector is well-suited to this study, which has the potential to provide the best measurement of $\sin 2\alpha$. Both calorimetry and particle identification are important in the reconstruction of $\rho^\pm\pi^\mp$ and the reduction of the continuum backgrounds. This study assumes small penguin contributions and neglects the interference between the channels.

The mass distributions of photon pairs obtained using the ASLUND Monte Carlo are shown in Figures 3-3(a) and (b) for the signal and light-quark continuum events, respectively. The low-mass tail of the π^0 peak is caused mainly by incomplete containment of showers as defined by the clustering algorithm, and possibly by longitudinal leakage from the back of the calorimeter. The peak of the signal distribution is offset slightly to the right of the nominal π^0 mass as a consequence of the combination of the low-energy tail and the resolution parameterization in ASLUND, which maintains the mean energy of clusters at the correct value.

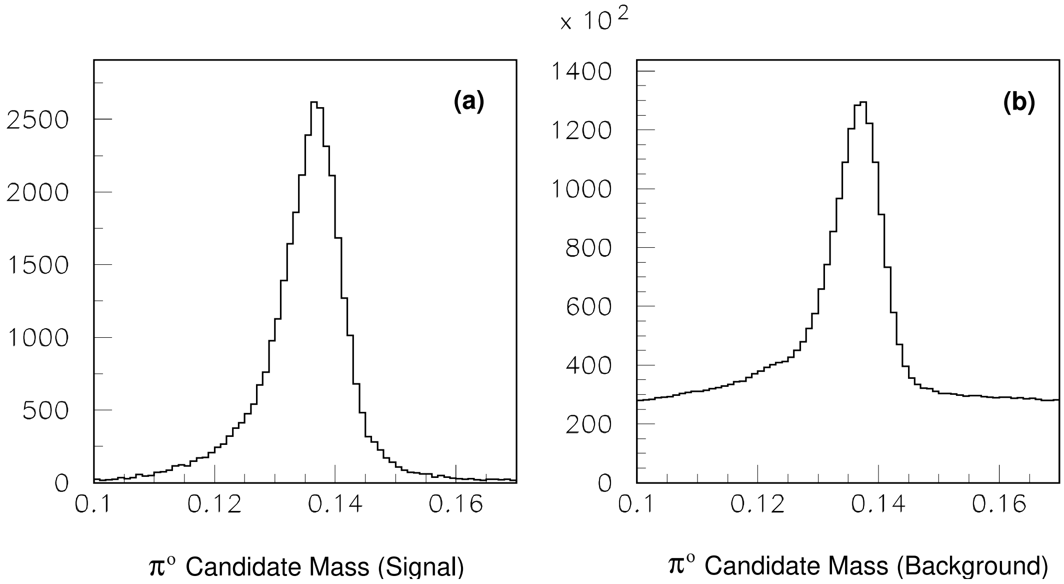

Figure 3-3. *Reconstructed two-photon mass for (a) signal and (b) light-quark background events.*

Candidate B^0s were reconstructed by combining $\rho^\pm$ candidates and all charged tracks of the opposite sign. Further cuts on the B^0-candidate momentum in the rest frame of the $\Upsilon(4S)$, and on its reconstructed mass, were made. These cuts have a dramatic effect on the backgrounds from all sources. The effects of all the above cuts on the signal are summarized in Table 3-15.

The fraction of continuum events that contribute a B^0 candidate to the background at this stage is 5.4×10^{-3}. Assuming a branching ratio of 5.8×10^{-5} for $B^0 \to \rho^\pm\pi^\mp$, we find that the continuum background dominates the signal by a factor of $\sim$140:1. A number of further cuts were made to reduce continuum backgrounds:

- All B^0 candidates were required to have a vertex within 5 cm of the nominal interaction point in the z direction. This excluded tracks from conversions and nonprompt decays with no appreciable effect on the signal.

- The two charged tracks from a B^0 decay to $\rho^\pm\pi^\mp$ were required to form a good vertex in three dimensions. In charm background events, the two charged tracks involved may arise from different charm decays and hence be well-separated in space. Candidates were therefore required to have a vertex χ^2 per degree of freedom less than 5.

- In the decay $B \to \rho^\pm\pi^\mp$, the ρ is 100% polarized, so that the angle of the decay axis with respect to its line of flight has a $\cos^2\theta_{decay}$ distribution. Background events,

Cut	Signal Efficiency
Geometry and $E_{min}(\gamma) = 25\,\mathrm{MeV}$	0.76
$111 \le m(\pi^0) \le 160\,\mathrm{MeV}/c^2$	0.98
Combined π^0 Efficiency	0.74
Geometry and $p_{t,min}(\pi) = 60\,\mathrm{MeV}$	0.91
$0.37 \le m(\rho) \le 1.17\,\mathrm{GeV}/c^2$	1.00
Combined ρ^{+-} Efficiency	0.91
Geometry and $p_{t,min} = 60\,\mathrm{MeV}$	0.96
B^0 Momentum in Υ Rest Frame	1.00
B^0 Candidate Mass	1.00
Overall B^0 Reconstruction Efficiency	0.65

Table 3-15. *Efficiencies of B^0 reconstruction for $\rho\pi$ modes.*

however, should show no such correlation. A cut was placed at $|\cos\theta_{decay}| \ge 0.25$ of the angle between the two directions in the ρ rest frame.

- More severe cuts were made on the B^0-candidate momentum in the $\Upsilon(4S)$ rest frame, and on its invariant mass.

- As in the $\pi^+\pi^-$ case, the light-quark background events have a pronounced jet structure, with the identified B-decay tracks lying within the jets. The thrust (or sphericity) axis of the remaining particles in the event is strongly correlated with the B-decay direction in background events and uncorrelated in signal events. Data are divided into six bins in $|\cos\theta_{thrust}|$ and all data is used to achieve maximum *CP*-sensitivity. Results for three of these bins are shown in the Table 3-16. For the best region, $|\cos\theta_{thrust}| \le 0.5$ a B/S of less than 3/2 is achieved with kaon tags, while with lepton tags this ratio is less than 0.15.

The efficiencies (and the relative tagging efficiencies) of the above cuts for signal and background are summarized in Table 3-16 along with the efficiencies for initial reconstruction, the branching ratios and cross sections, and finally, the overall background contamination per reconstructed B meson. Unbracketed numbers correspond to kaon tags, bracketed ones to lepton tags. A multivariate analysis has also been performed, following the lines of Reference [Ale91], and leads to similar results.

Cut	Signal	Light Quark	Charm
Reconstructions and Preliminary Cuts	0.65	6.70 $\times 10^{-3}$	3.20 $\times 10^{-3}$
$\lvert Z_{vert}\rvert < 5\,\mathrm{cm}$	1.00	1.00	1.00
Chi-squared per d.o.f. of Vertex	0.98	0.92	0.68
$\lvert cos\theta_{decay}\rvert > 0.25$	0.98	0.85	0.87
$0.14 \leq p(B^0) \leq 0.44\,\mathrm{GeV}/c$	0.98	0.42	0.42
$5.20 \leq m(B^0) \leq 5.36\,\mathrm{GeV}/c^2$	0.95	0.31	0.30
Tagging Efficiency w.r.t. Signal	1.0(1.0)	0.47(0.049)	1.4(0.065)
One candidate per event	1.0	0.77	0.68
Efficiency for $0.0 < \lvert cos\theta_{thrust}\rvert < 0.5$	0.29	1.13(0.117) $\times 10^{-5}$	0.69(0.031) $\times 10^{-5}$
Efficiency for $0.7 < \lvert cos\theta_{thrust}\rvert < 0.8$	0.058	1.65(0.170) $\times 10^{-5}$	1.98(0.089) $\times 10^{-5}$
Efficiency for $0.9 < \lvert cos\theta_{thrust}\rvert < 1.0$	0.058	16.0(1.65) $\times 10^{-5}$	13.5(0.611) $\times 10^{-5}$

Table 3-16. *Example of background rejection cuts for $\rho\pi$ modes. Unbracketed numbers correspond to kaon tags (class b), bracketed ones to lepton tags (class a). Data samples in higher $\lvert\cos(\theta_{thrust})\rvert$ bins have higher backgrounds.*

3.7 Tagging Modes

Measurements of *CP* asymmetries and B^0 or B_s mixing require the determination of the B flavor. At BaBar, events are studied in which a coherent $B^0\overline{B}^0$ state produces one B meson decaying into a mode under investigation for *CP* violation, while the flavor of the second B is reconstructed (or tagged) from its decay products. Any particle with a distinct flavor quantum number provides a possible tag. Typically this information is in the form of a lepton charge, a D charge, or a K charge.

The observed asymmetry $a_{obs}(t)$ can be related to the expected asymmetry, a_{theory}, by

$$a_{obs}(t) = D \cdot a_{theory}(t) \tag{3.15}$$

with a dilution factor $|D| < 1$, where $D = (1 - 2w)$, and w is the wrong-tag probability. (The further dilution effect of smearing due to limited time resolution is discussed in the following section.) Different types of tagging information in a single event are combined, leading to an event-by-event definition of the appropriate dilution factor.

Details of the most recent tagging studies are discussed in References [Wal95] and [Pla95]. The results are similar. The numbers reported here are taken from the first of these studies, which uses a Monte Carlo simulation based on a version of the event generator JETSET 7.4 [Sjo93] tuned to reproduce ARGUS data [Alb94*b*]. This study builds on earlier work which identified a number of effective tagging strategies [Jaf94, Wal94*a*, Pia94]. The strategy is to use all possible information in each event to assign the appropriate flavor and dilution factor, and then to extract asymmetries from a two-dimensional fit of the data against time and effective dilution. The detector acceptance, momentum and energy resolution, and particle identification are simulated with ASLUND.

A flavor estimator that allows us to combine all tagging information in an event is assigned as follows. For each event, find all possible tagging identifiers. For each identifier, calculate the quantities L_i, Q_i, and D_i and define $B_i = L_i \cdot D_i \cdot Q_i$. The likelihood ratio L_i, which estimates whether the tagging track is correctly identified as a particle of type i, is given by

$$L_i = \frac{e^{-\chi_i^2/2}}{\sum_{j=e,\mu,\pi,K,p} e^{-\chi_j^2/2}}, \tag{3.16}$$

where χ_i^2 is the sum of the χ^2 from each available source of information for particle type i. The flavor charge Q_i for a track of type i is defined to be $+1$ for a B^0 right-sign tag and -1 for the opposite sign. Right sign is defined below for each class of decays. The appropriate dilution factor for D_i for this particular tag type and event characteristics is then calculated from the simulation. Eventually, these numbers will also be checked by the study of events in which both B mesons decay to tagging modes. For each event a combined flavor estimator is defined as follows: for events with more than one possible tagging identifier, the B_i are added like relativistic velocities (v/c) to give a $\hat{B}$, such that $-1 \leq \hat{B} \leq 1$; for events with only one identifier, $\hat{B} = B_1$. If the single estimators were statistically independent, $\hat{B}$ would be equal to the effective dilution D_{eff} for that event. In fact, they are not fully independent, but one can measure $D_{eff}(\hat{B})$ using doubly tagged modes [Wal95]. A cut on $\hat{B}$ provides a simple way to select against poor tags using all the information in the event. A two-dimensional fit to the asymmetry against time and $\hat{B}$ does not require such a cut and thus has slightly higher tagging performance. Other studies [Pla95] use a slightly different approach to combining all possible tagging information, directly defining an effective wrong tag fraction x_{eff} for each event rather than introducing $\hat{B}$.

3.7.1 Kaon Tags

The sign of a kaon's charge is a signature of its strangeness. The principal sources of Ks from b-quark decay are:

$$\begin{array}{ll}
b \to cW^-; c \to W^+ s, s \Rightarrow K^-, & \text{(a)} \\
b \to XW^-; W^- \to \overline{c}s, s \Rightarrow K^- \text{ and/or } \overline{c} \to W^+\overline{s}, \overline{s} \Rightarrow K^+, & \text{(b)} \\
b \to cW^-; W^- \to \overline{u}s, s \Rightarrow K^- \text{ and/or } c \to XW^+, W^+ \to u\overline{s}, \overline{s} \Rightarrow K^+, & \text{(c)} \\
b \to Xs\overline{s}; s \Rightarrow K^- \text{ and/or } \overline{s} \Rightarrow K^+, & \text{(d)} \\
b \to sq\bar{q} \text{ } (penguin); s \Rightarrow K^-. & \text{(e)}
\end{array}$$

We call the K from the dominant process (a) the right-sign kaon. Thus, $Q_K = +1$ for a K^+ and -1 for K^-. Processes (b), (c), and (d) yield both right-sign and wrong-sign kaons, typically with a second strange particle in the event. Doubly Cabibbo-suppressed and penguin processes (e) give tiny contributions. Events with multiple like-sign kaons can occur since the processes listed above are not mutually exclusive. Wrong-sign particles contribute to the wrong-tag probability, but as the list above shows, other characteristics of the event can be used to reduce the wrong-tag fraction. Aside from the presence or absence of a second K in the event and its charge, the wrong-tag fraction also depends somewhat on the kaon momentum in the $\Upsilon(4S)$ rest frame.

Kaons are identified via dE/dx by the DIRC in the barrel, and by aerogel Cherenkov counters in the forward endcap. This information is combined into a likelihood. Tracks with $L_K > 0.5$ are counted as charged kaons in assigning event classes. All Ks with $L_K > 0.1$ contribute to the determination of $\hat{B}$. In this simulation, kaons which decay before reaching the DIRC do not contribute. This is a conservative assumption, since dE/dx information or the geometric signature of a kaon decay in flight may in fact lead to the recovery of good kaon identification in some cases.

On the basis of the simulations described above, the performance of all kaon tags (with or without leptons) is $\epsilon_K D^2_{eff} = 0.21$. Here, ϵ_K is the kaon tagging efficiency, that is, the fraction of generic B^0 decays for which a kaon tag is available.

3.7.2 Lepton Tags

Electrons and muons in b decays come from several sources:

$$b \to XW^-; W^- \Rightarrow l^-, (0.105e + 0.105\mu),\ W^- \to \tau^- \Rightarrow l^- \ (\sim 0.005e + 0.005\mu), \quad \text{(a)}$$
$$b \to Xc; c \to XW^+, W^+ \Rightarrow l^+ \ (\sim 0.09e + 0.09\mu), \quad \text{(b)}$$
$$b \to \overline{c}cs; \overline{c} \to XW^-W^- \Rightarrow l^- \ (\sim 0.01e + 0.01\mu), \quad \text{(c)}$$
$$b \to \overline{c}cs; \overline{c}c \to J/\psi \, or \, J/\psi', J/\psi \Rightarrow l^+l^- (\sim 0.003e + 0.003\mu). \quad \text{(d)}$$

The lepton from a semileptonic B decay, process (a), is defined as a right-sign lepton. Process (d) is a tiny source of spurious tags when one or the other lepton is missed. Each decay path leads to a distinct distribution in the lepton momentum, the number and invariant mass of the other accompanying particles, and the distribution of the remaining energy with respect to the lepton direction [Jaf94, Pia94]. All such information is used, when available, to determine the wrong-tag fraction. For example, Figure 3-4 shows the distributions of right- and wrong-sign leptons as a function of momentum, p^*, in the $\Upsilon(4S)$ rest frame. At low momentum, wrong-sign leptons dominate and can contribute usefully to tagging.

Electrons are identified in the electromagnetic calorimeter and at low momenta by the DIRC and dE/dx measurements. Muons are identified in the IFR supplemented by DIRC at low

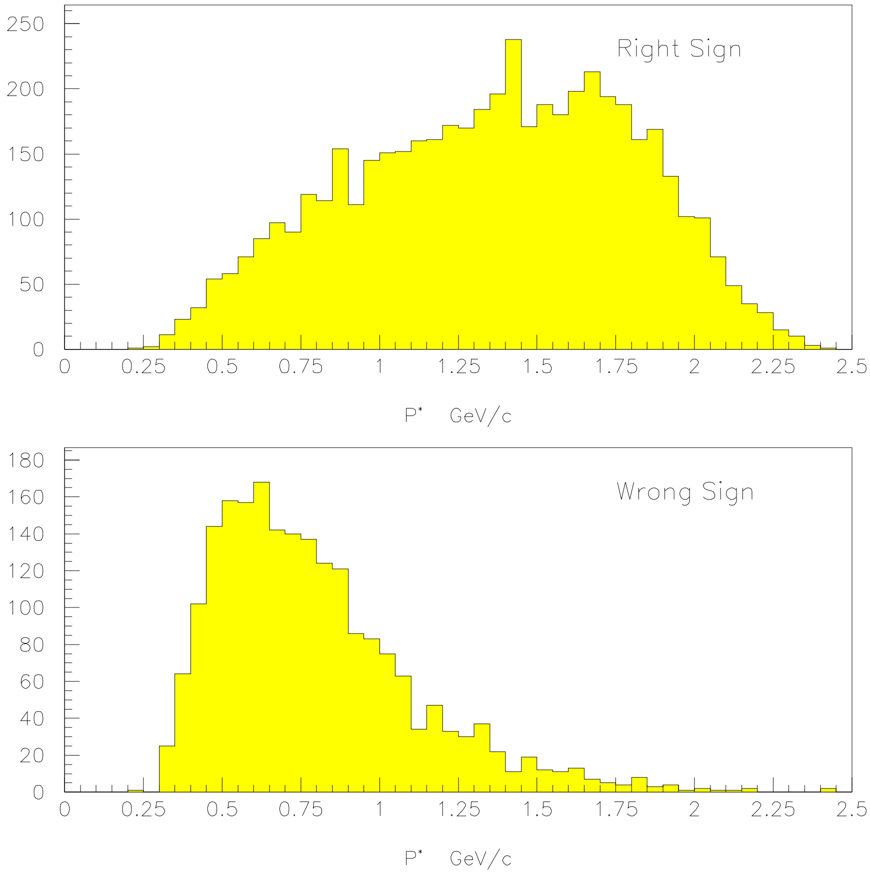

Figure 3-4. *Distribution of momentum in the $\Upsilon(4S)$ rest frame for leptons. Right-sign leptons are l^+ for B^0 decays and l^- for $\overline{B}^0$.*

momenta. In low momentum regions, where the separation from hadrons is not perfect, each candidate is weighted by its likelihood, and cuts at $L_e > 0.7$ and $L_\mu > 0.7$ are applied.

We take the semileptonic branching fraction of the B^0 meson to be 10.5%. Simulations of the lepton tagging performance give $\epsilon_l D^2_{eff} = 0.13$. Here, ϵ_l is the lepton tagging efficiency, that is, the fraction of signal events with an identified lepton tag. The performance number includes a cut $|\hat{B}| > 0.4$. A two-dimensional fit to the asymmetry, binning the data in time and in $\hat{B}$, gives slightly higher tagging performance, $\epsilon_l D^2_{eff} = 0.16$.

Class	Selection Efficiency (ϵ)	Efficiency ($\hat{B} \geq 0.1$)	Performance (ϵD^2_{eff})
A	0.20	.19	0.13
B	0.80	.66	0.21
All	1.0	0.86	0.34

Table 3-17. *Performance figures for lepton and kaon tags and for combined tagging using all events.*

3.7.3 Other Tags

In addition to lepton and kaon tags, charged pions have a significant flavor correlation at the high end of the momentum spectrum due to two-body decays with a charged π or ρ meson, and at the low end due to pions from $D^{*+} \to \pi^+ D^0$ [Sny90]. Additional D tags can be formed from neutral Ks. Strange baryons, though rare, provide a small contribution to tagging. These effects are included in the analysis presented here. Ongoing studies continue to identify further ways of reconstructing events that can lead to a flavor assignment with a non-negligible D_{eff}. All such information will be used to maximize tagging performance.

3.7.4 Combined Tagging

All available information is used to calculate a combined tagging performance factor $\hat{B}$ for each event, thus creating a two-dimensional distribution in time and the effective dilution $D_{eff}(\hat{B})$ (or equivalently x_{eff}) to be used in fitting for the asymmetry. We divide tagged events into two classes, class A being those events with a lepton which has a high probability of being a primary lepton from semileptonic B decay, and class B being all other events. This separation is necessary because the vertex resolution for the tagging decay is different for the two cases, and hence the contribution to a *CP*-asymmetry measurement must be determined separately for each case. More precisely, class A includes events containing either: (1) a lepton with $p^* > 1.4\,\mathrm{GeV}/c$; or (2) a lepton with $p^* > 0.5\,\mathrm{GeV}/c$, and no other charged tracks or a total energy of less than $0.5\,\mathrm{GeV}$ within the same hemisphere in the $\Upsilon(4S)$ rest frame. The results are given in Table 3-17. The efficiency values include misidentified particles, but the effective dilution factors correct for this. The quantity labeled "performance" is defined to be the sum over bins with $\hat{B} \geq 0.1$ of ϵD^2_{eff}, where ϵ is the fraction of signal events in the bin. If the lepton information alone were used for class A events, the performance would be only 0.125; the higher combined performance listed in the table shows the impact of the additional information on these events.

3.8 Estimate of *CP*-Angle Measurement

3.8.1 Method of Calculation

Using the approximation that both Bs have a boost equal to β, namely the boost of the $\Upsilon(4S)$, the quantity $\Delta z = z_{cp} - z_{tag}$ is related to the time difference between the two B decays by:

$$t = \frac{\Delta z}{\beta\gamma}.$$

Based on the simulations described above, each *CP* analysis channel (loosely called a *CP* mode in the following) and each tagging class, are characterized by efficiency, background (or dilution for tags), and z resolution. For each *CP* mode and tagging class, the distribution in time and b flavor is regenerated from these parameters. The program CPEXTRACT [Sny94] is then used to perform a binned maximum likelihood fit to this data and to make an estimate of the error on the asymmetry for a sample corresponding to $30 fb^{-1}$ of $\Upsilon(4S)$ data. This fit includes the dependence on time, tagging type, and background. Errors are quoted for zero *CP* asymmetry, since our sensitivity to small asymmetries is the quantity of interest. More details of the calculation are given in Reference [Sny95].

The Δz resolution of background events (such as those that occur in the $\pi^+\pi^-$ and $\rho\pi$ analyses) is treated separately in CPEXTRACT. This enhances our ability to discriminate against these backgrounds since the background events are produced at $\Delta z = 0$, and the resolution on Δz is better for background events than for signal plus tag events. The resolutions on Δz for $\rho\pi$ backgrounds can be parameterized by two Gaussian distributions, with 90% of the events in a narrow component ($\sigma_{narrow} = 80\,\mu$m) and the remaining events in the wide component ($\sigma_{wide} = 280\,\mu$m). Furthermore, since the expected asymmetry behaves as $\sin(K\Delta z)$, where $K = \delta M/\beta\gamma c$, the impact of background on the fitted asymmetry parameters is minimized by correct treatment of the Δz dependence. This is illustrated by Figure 3-5 which shows the Δz distribution for $B \to \rho\pi$ with a class B (mostly kaon) tag, an assumed asymmetry of 0.866 ($\beta = 30°$), and an assumed background-to-signal ratio of 9. As can be seen, the background drops significantly by the time the asymmetry develops. The improvement in *CP*-resolution obtained by explicitly fitting for the Δz dependence of the background is shown in Figure 3-6.

Here, wrong-sign tags are assumed to have the same Δz distribution as right-sign tags. This is a pessimistic assumption because, in general, the wrong-sign Δz distribution will be significantly broader, which will tend to reduce the adverse effects that they have on the time-dependent asymmetry. In the final analysis, they must be handled correctly, or a significant systematic error will be introduced.

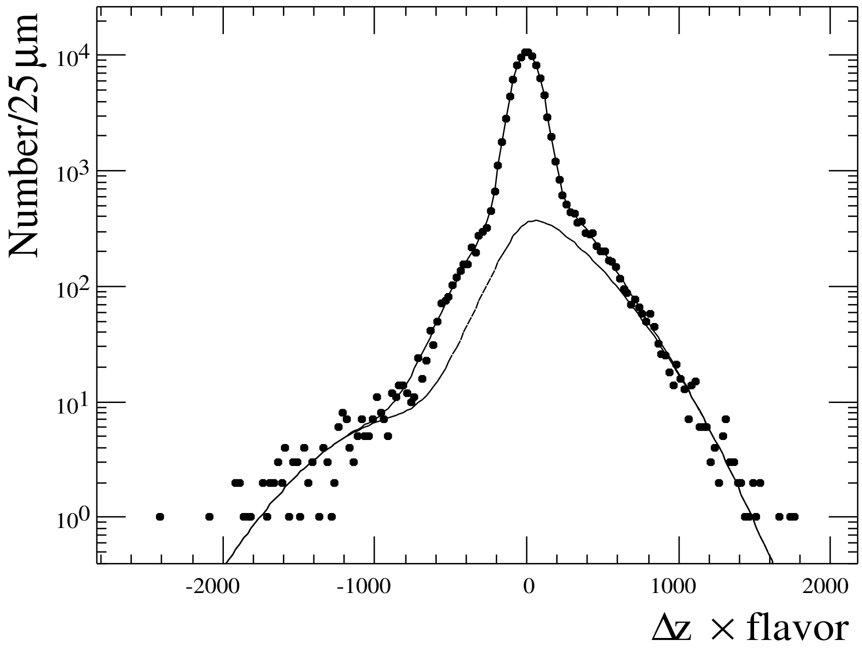

Figure 3-5. *Distribution of Δz for the CP-state $\rho\pi$ using class B tag and an assumed background-to-signal ratio of 9.*

For lepton tagged events, there is a strong dependence of the Δz resolution on polar angle. This is accounted for by the simple expedient of dividing the direct lepton tag into two polar angle bins and treating each bin as an independent tag. Further refinement of this treatment can no doubt be used to improve accuracy in the actual data analysis.

3.8.2 Tagging Modes

For tagging efficiencies, we use the numbers given in Table 3-17 above. For both class A and class B tags, we estimate the z coordinate of the tag by fitting a common vertex to all tracks except those associated with the *CP*-state and those with transverse impact parameter greater than 1 mm. This last effectively excludes the decay products of kaons, lambdas, *etc.* Since the z resolution depends strongly on the direction of the tagging track [Cha95], the tags are divided into seven bins based on the tangent of the dip angle ($|tan\theta_{dip}|$) in order to optimize our *CP*-sensitivity. The numbers used in this document were obtained from a high statistics ASLUND simulation. Details can be found in [Wea95]. BBSIM simulations [Cha95] confirm these results for lepton tags.

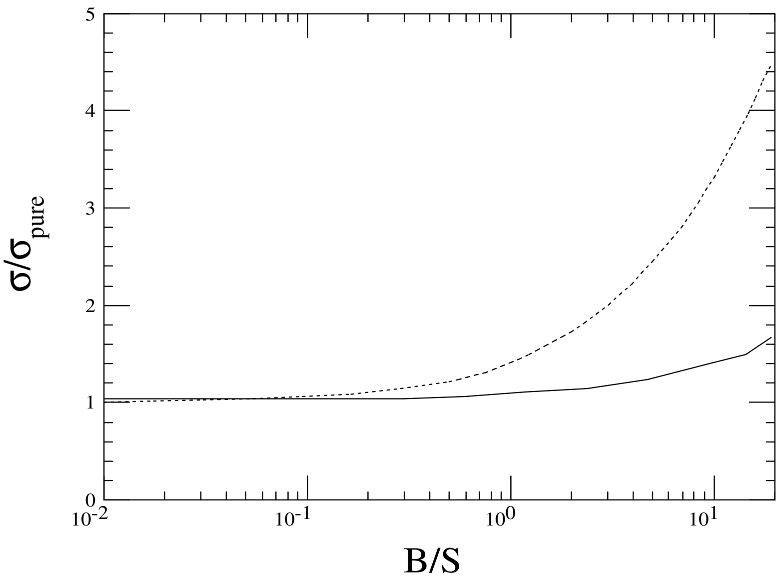

Figure 3-6. *Ratio of σ_{cp} in the presence of background to σ_{cp} obtained without background as function of the background-to-signal (B/S) ratio. The solid curve corresponds to fitting for the Δz dependencies of the background and the signal. The dashed curve results if Δz information is not exploited.*

3.8.3 *CP* Modes

The parameters required to determine sensitivity (branching fractions, number of events expected, backgrounds, and z_{CP} resolutions) for each *CP*-mode under consideration are compiled in Table 3-18. These results are collected from the studies described above. The expected number of events before tagging is based on $30 fb^{-1}$ collected on the $\Upsilon(4S)$. The z resolutions for each mode are characterized by three numbers: σ_{narrow}, σ_{wide}, and the ratio of the area of the narrow Gaussian to the wide one. For D^+D^-, many decay modes contribute, and events are grouped into two classes, four-prong and six-prong decays. A single Gaussian then gives an adequate parameterization of the z resolution of D^+D^- events in each class. Similarly, for $D^{*+}D^{*-}$ decays, events are classified by the number of π^0s in the final state, and then a single Gaussian suffices to characterize the z resolution of each class.

For $J/\psi K_L$ the background consist of two components: a *CP* symmetric part (the first number) and a *CP* anti-symmetric part given in parenthesis. For all modes with background the number in square brackets gives the degradation in σ_{cp} that results from the background. Our procedure of estimating the *CP*-violating asymmetry by dividing the data into samples with varying background levels and fitting explicitly to the Δz distribution of the background

Mode	Branching Fraction	Usable Sample	Efficiency	Reconstructed Number	Background	z Resolution
$J/\psi K^0_S$	0.5×10^{-3}	2160	0.41	1106	negligible	36/111/16
$J/\psi K^0_L$	0.5×10^{-3}	2160	0.33	712	191(96)[1.3]	36/111/16
$J/\psi K^*$	1.6×10^{-3}	788	0.39	307	negligible	37/155/10
D^+D^-	6×10^{-4}	993	0.25	248	109 [1.02]	52(6-prongs)
						75(4-prongs)
$D^{*+}D^{*-}$	7×10^{-4}	3130	0.155	485	62 [1.005]	43 (0 π^0)
						51 (1 π^0)
						69 (2 π^0)
$\pi^+\pi^-$	1.2×10^{-5}	432	0.80	346	1957 [1.11]	34/161/4.4
$\rho^\pm\pi^\mp$	5.8×10^{-5}	2088	0.56	1162	33420 [1.18]	36/240/24

Table 3-18. *Simulated efficiencies, backgrounds, and vertex resolutions for CP modes. The usable sample reflects the visible branching ratio and the 30 fb^{-1} sample size. Reconstructed number of events does not include tagging efficiencies. The background number given is for the total sample; in the analysis the data are divided into bins of varying background to minimize the adverse impact on CP resolution. The factor by which background actually degrades the resolution is given in square brackets.*

when estimating the CP-violating asymmetry gives a substantial improvement in sensitivity over a naive treatment which uses a factor of $\sqrt{1+B/S}$.

The resolution on the CP-violating phase $(\phi_M - \phi_D)$ for each CP state is given in Table 3-19. The combined sensitivity for $\sin 2\alpha$ and $\sin 2\beta$ is estimated to be ± 0.059 and ± 0.085, respectively, for 30 fb^{-1}, or one year's data at nominal luminosity. The channels $J/\psi K^*$, D^*D, D^*D^*, $\rho\pi$, and $a_1\pi$, which are not pure CP eigenstates, are assumed to be dominated by a single CP eigenstate. If this is not the case, the resolution obtained with these modes will be reduced. An accuracy on the CP phase comparable to the DD modes can be expected. The results in this table differ in many ways from those given in the *Letter of Intent*. The differences arise from two major sources. First, our knowledge of the branching ratio to the modes of interest has improved somewhat, resulting in changes in these key input numbers. Second, more complete simulation work, including backgrounds, has been carried out for most of the channels included in Table 3-19, resulting in changed efficiencies and signal-to-background ratios. The number given for the $a_1\pi$ channel is an estimate based on the work of Reference [Ale91]. The number obtained in that paper has been rescaled, reflecting the integrated luminosity assumed here, using the tagging efficiency expected for this detector, and correcting the assumed branching fraction for $B \to \pi\pi$. For the D^*D channel, the estimate is based on the simulations of the DD and D^*D^* channels and the measured $B \to D_s D^*$ branching ratios.

CP State	Br	$\phi_M - \phi_D$	A Tags	B Tags	Combined
$J/\psi K_S^0$	0.5×10^{-3}	β	0.15	0.13	0.098
$J/\psi K_L^0$	0.5×10^{-3}		0.25	0.21	0.16
$J/\psi K^*$	1.6×10^{-3}		0.29	0.25	0.19
D^+D^-	6×10^{-4}	β	0.32	0.27	0.21
$D^{*+}D^{*-}$	7×10^{-4}		0.24	0.20	0.15
$D^{*\pm}D^{\mp}$	8×10^{-4}				0.15*
Combined		β			0.059
$\pi^+\pi^-$	1.2×10^{-5}	α	0.29	0.27	0.20
$\rho\pi$	5.8×10^{-5}		0.16	0.16	0.11
$a_1\pi$	6×10^{-5}				0.24*
Combined		α			0.085

Table 3-19. *Error on the measurement of* $(\phi_M - \phi_D)$ *from various channels for 30* fb^{-1}. *The A-tag sample is chiefly direct leptons, and the B sample is all other tags. The numbers marked * ($a_1\pi$ and D^*D) are estimates; all others are based on simulations.*

The accuracy achievable for the $\rho\pi$ channel depends on the ratio $R = \Gamma(B^0 \to \rho^+\pi^-)/\Gamma(B^0 \to \rho^-\pi^+)$ [Ale91, Ale93]. The results given in Table 3-19 assume $R = 1$. The dependence of the sensitivity on this assumption is shown in Figure 3-7.

3.9 CKM Matrix Determination

The values of the CKM matrix elements determine the lengths of the sides of the unitarity triangle. Accurate measurements of these elements are thus an important ingredient in overconstraining the triangle and probing the source of *CP* violation. Furthermore, the values of the CKM elements are fundamental input parameters within the Standard Model and hence, must be measured as precisely as possible; better knowledge of these parameters may provide some insight into their origin. The present status of these elements is summarized in Figure 3-8 in the Wolfenstein parameterization, where the shaded area is that allowed in the Standard Model for the apex of the unitarity triangle in the (ρ, η) plane. The parameters used for the plot of the allowed region for the unitarity triangle are taken from the draft of a Review of Modern Physics article by P. Burchat and J. Richman [Ric95]. The two directly-measured CKM parameters are $|V_{cb}| = 0.040 \pm 0.003$ and $|V_{ub}/V_{cb}| = 0.076 \pm 0.026$. The value of the parameter that describes B_d^0-$\overline{B}_d^0$ mixing is $\Delta m(B^0) = x_d/\tau_{B^0} = 0.43 \pm 0.06\,\mathrm{ps}^{-1}$. The top quark mass evaluated at the relevant scale for this mixing is $m_t = 165 \pm 15\,\mathrm{GeV}$. The hadronic matrix elements obtained in lattice calculations are $f_B\sqrt{B_B} = 200 \pm 40\,\mathrm{MeV}$, and $B_K = 0.75 \pm 0.05$. The resulting errors are added in quadrature, and the lines shown

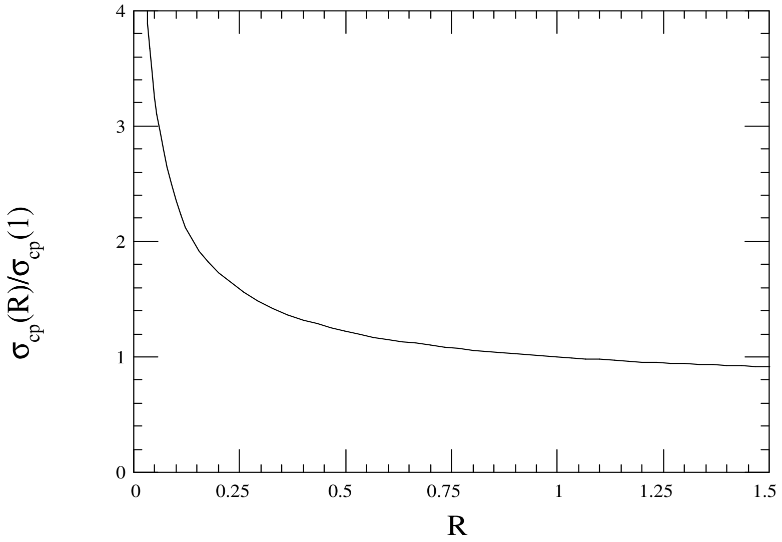

Figure 3-7. *Dependence of the error on the CP asymmetry angle α on the assumed value for the ratio of decay widths $R = \Gamma(B^0 \to \rho^+\pi^-)/\Gamma(B^0 \to \rho^-\pi^+)$, normalized to the case $R = 1$.*

in the plot correspond to $\pm 1.5\sigma$ limits. The overlapping limits result in the following set of allowed ranges for the unitary angles:

$$\begin{aligned} -0.59 \leq &\ \sin 2\alpha \ \leq 1.0 \\ 0.29 \leq &\ \sin 2\beta \ \leq 0.88 \\ -1.0 \leq &\ \sin 2\gamma \ \leq 1.0\,. \end{aligned} \tag{3.17}$$

It is important to remember that this picture represents the Standard Model and can be dramatically altered if new physics is present. Examples include new contributions to ϵ or B_d^0-$\overline{B}_d^0$ mixing, even if no new sources of *CP* violation are present. It is equally important to note that, since the range of values of parameters such as B_K and B_B is constrained by theory rather than experiment, the overlap region is a best estimate rather than a 90% confidence level result.

3.9.1 V_{cb}

Values for V_{cb} are extracted from the investigation of inclusive and exclusive semileptonic B decays. CLEO and LEP have determined V_{cb} at the 7.5% level [Ric95], depending on the

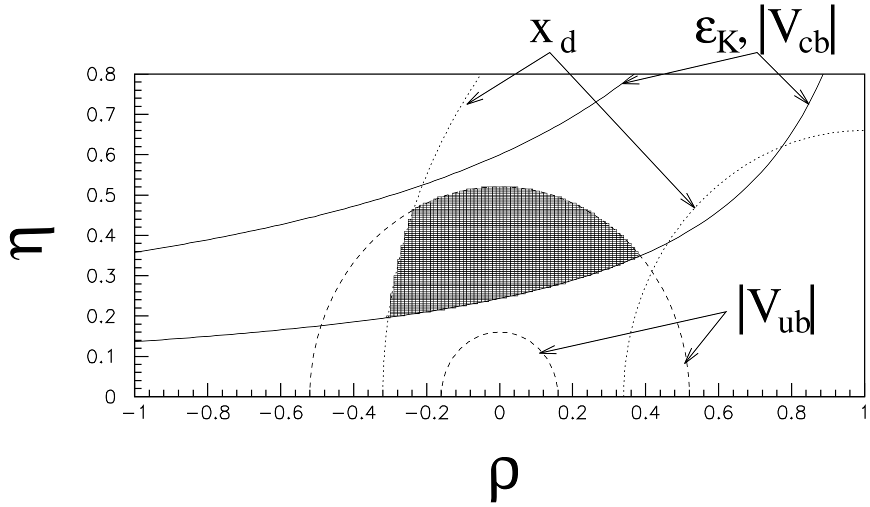

Figure 3-8. *Constraints in the Standard Model in the $\rho\eta$ plane. The shaded area corresponds to that allowed for the apex of the rescaled unitarity triangle.*

extraction technique, and BaBar can expect to reduce these errors to the few percent level due to the expected large data sample and efficient reconstruction techniques. The inclusive semileptonic branching fraction B_{SL} can be determined from:

1. Measurement of the inclusive single-lepton momentum spectrum. This technique yields significant data samples, but the procedure used to fit the observed spectrum to the expected shape for primary and secondary leptons from B and charm decay, respectively, introduces a large model dependence.

2. Charge and angular correlations in dilepton events. This offers less model dependence, as the measured correlations can be used to separate the primary and secondary lepton spectra, instead of relying on theory.

3. Separate measurement of B_{SL} for charged and neutral B meson decay. Here, one B in the event must be reconstructed in order to tag the charge of the other; this will require the large tagged event sample available to BaBar.

Determination of V_{cb} from B_{SL} via technique (1) at CLEO and LEP is already dominated by the theoretical error, while method (2) still offers room for improvement on the systematic and statistical errors. In addition, it is important to make better measurements of B_{SL} for the charged and neutral B mesons separately. These are used to determine the ratio of B lifetimes, which in turn are used in interpreting exclusive semileptonic and hadronic decay rates. In these measurements, one B in the event is reconstructed in order to tag the charge of the other; this will benefit from the large tagged event sample available to BaBar.

Exclusive semileptonic decays offer a reliable model-independent determination of V_{cb} within the framework of heavy quark effective theory (HQET). The heavy quark symmetry allows the normalization of the q^2-dependent hadronic form factors with good precision at zero recoil for the charm hadron system. This technique is best suited for the process $B \to D^* \ell \nu_\ell$ as the leading corrections to the HQET result arise only at higher order, $1/m_Q^2$. Due to the presence of the neutrino, reconstruction of exclusive semileptonic channels is more difficult than for hadronic decays; at present, the $B \to D^* \ell \nu_\ell$ mode is the most precisely measured. One technique at the $\Upsilon(4S)$ is to determine the missing momentum distribution recoiling against the $D^* \ell$ system. The zero recoil configuration for the charm hadrons results in a reduction of phase space for the decay (as the B and D^* mesons have approximately equal velocities), yielding a statistically limited data sample, and requires good detection efficiency for low momentum pions arising from the D^* decay. Measurements of other exclusive modes, such as $D \ell \nu_\ell$ and $D^{**} \ell \nu_\ell$, will also be precisely studied at *BaBar*.

3.9.2 V_{ub}

An accurate determination of V_{ub} is important to test closure of the unitarity triangle. Data near the end-point region of the lepton momentum spectrum in inclusive semileptonic B decays have established that V_{ub} is nonzero. However, converting the measured rate into a value of V_{ub} introduces substantial errors. This conversion is highly model dependent due to the small phase space available at the end-point, the large uncertainties in the calculation of the rates for the resonant modes, and the relative sizes of the contributions of resonant and nonresonant modes in this region. The subtraction of background from the small data sample is an additional large source of error. The present experimental error on the ratio $|V_{ub}|/|V_{cb}|$ is comparable to the theoretical uncertainty, and thus new, less model dependent techniques for extracting this CKM element are necessary.

Measurement of exclusive semileptonic decays ($B \to X_u \ell \nu_\ell$, where $X_u = \pi, \rho$, or ω) requires a large data sample and should provide an improved determination of V_{ub}. Such decays have yet to be observed, but model predictions indicate that the rate should be distributed over many exclusive channels, with no dominant modes. The theoretical uncertainties are expected to be lower than in the inclusive case. Further reductions in the theoretical errors can be obtained via measurements of the form factor q^2 distributions in $c \to d$ transitions such as $D \to X_u \ell \nu_\ell$. Given adequate statistics and understanding of experimental systematics from vertex separation and π/K identification, such form factor measurements can be made at *BaBar*.

An alternative method [Bar90] of extracting V_{ub} from semileptonic B decays is to measure the invariant mass spectrum of the final state hadrons *below* the charm hadron threshold, *i.e.*, $m_X < m_D$. A study of this method at BaBar has yet to be made, but the advantages of separate vertexing of the two Bs will probably be important for this technique to be feasible.

3.9.3 V_{td}

It has recently been shown [Atw94, Gol94, Des94] that the proposed method of obtaining the ratio $|V_{td}/V_{ts}|^2$ from the ratio of branching fractions $B(B \to \rho\gamma)/B(B \to K^*\gamma)$ is not valid due to the potentially large long-distance contributions to these exclusive B decay modes. The sizes of these long-distance contributions could be determined with a measurement of exclusive radiative charm decays, such as $D \to \rho\gamma$, which are expected to have no short-distance contamination. Separate measurements of $B^- \to \rho^-\gamma$ and $B^0 \to \rho^0\gamma$ as well as $B_s \to \phi\gamma, K^{*0}\gamma$ may also provide an estimate of the long-distance rates.

A measurement of B_s^0-$\bar{B}_s^0$ mixing could also yield a value for this ratio of CKM elements as

$$\frac{x_s}{x_d} = \frac{m_{B_s}\eta_{QCD}^{B_s} B f_{B_s}^2 |V_{ts}|^2}{m_{B_d}\eta_{QCD}^{B_d} B f_{B_d}^2 |V_{td}|^2} = \xi_s^2 \frac{1}{\lambda^2[(1-\rho)^2+\eta^2]} . \tag{3.18}$$

The factor ξ_s, which multiplies the ratio of CKM elements, measures the amount of $SU(3)$ breaking effects and is estimated to be 1.3. Determination of $f_{B_{(s)}}$ from the decay $B_{(s)} \to \tau\nu_\tau$ will greatly reduce the theoretical uncertainty in this mixing ratio. The allowed region of the $\rho\eta$ plane, determined above in the Standard Model, yields x_s = 10–57. A precise measurement of B_s mixing requires a substantial run on the $\Upsilon(5S)$. It is needed in order to obtain a clean determination of $|V_{td}|/|V_{ts}|$. If V_{ts} is relatively large, a more accurate value of $|V_{td}/V_{ts}|^2$ could be obtained from a measurement of $\Delta\Gamma/\Gamma$ for the B_s meson [Bro95].

3.10 Rare B Decays

Rare B decays are an important testbed of the Standard Model. They offer a complementary strategy in the search for new physics by probing the indirect effects of new interactions in higher order processes. In particular, the probing of loop-induced couplings can provide tests of the detailed structure of the Standard Model at the level of radiative corrections, where the Glashow-Iliopoulos-Maiani cancellations are important. The recent observation of radiative B decays by CLEO has already provided bounds on the CKM ratio $|V_{ts}/V_{cb}|$ as well as powerful constraints on new physics. The high luminosity and separated B vertices available at PEP-II and improved particle identification capabilities of BaBar will be needed to allow accurate measurements of many rare modes. No full detector study has yet been made for any of these channels. However, BABAR is designed to give as complete information on all tracks as can reasonably be achieved, and hence, is well-suited to extend our knowledge of these modes.

3.10.1 $B \to \tau\nu$

The decay $B \to \tau\nu$ is of interest because the branching ratio will yield a value of the product $f_B^2|V_{ub}|^2$. The general expression for the decay width for the decay $B \to \ell\nu$ is

$$\Gamma(B^+ \to l^+\nu) = \frac{G_F^2}{8\pi} f_B^2 m_B m_l^2 |V_{ub}|^2 \Big(1 - \frac{m_l^2}{m_b^2}\Big)^2,$$

where G_F is the Fermi constant, f_B is the B-meson coupling constant, m_B is the mass of the B meson, m_l is the lepton mass, and V_{ub} is the CKM-matrix element. For the decay $B \to \tau\nu$, the branching ratio is about 8×10^{-5}.

Leptonic decays of the B meson are expected to be best identified by fully reconstructing one charged B meson (the tagging B) in events in which the only observed particle coming from the decay of the second B meson is a charged lepton. The separation of the decay vertices of the two B mesons, along with the excellent mass resolution of the detector, allows an unambiguous identification of the tagging B meson. The problem then is to reject decays of the nontagging B mesons which are not purely leptonic but in which only a single lepton is identified in the detector. A classic example of this type of decay is the semileptonic decay $B \to \ell K_L^0 \nu$, in which neither the ν nor the K_L^0 are detected. The BABAR detector needs to have excellent muon and K_L^0 detection and rejection capabilities in order to veto these types of decays with high efficiency.

For the decay $B \to \mu\nu$, the branching ratio is about 4×10^{-7}, a factor of 200 smaller than that for $B \to \tau\nu$. However, $B \to \mu\nu$ decays should be much easier to detect and discriminate from backgrounds because they are two-body decays, and hence the muons are close to monoenergetic. Further Monte Carlo simulation work needs to be done before a prediction can be made of the level of sensitivity of the BABAR detector to $B \to \ell\nu$ decays and to determine whether $\tau\nu$ or $\mu\nu$ searches give better sensitivity. However, it is already clear that the general design of the detector and the separate vertexing of the two Bs make BABAR competitive with any other experiment for this search.

3.10.2 $B \to X_s \ell^+ \ell^-$

This decay receives short-distance contributions from electromagnetic and Z^0 penguin diagrams as well as W box diagrams, and long-distance contributions from the process $B \to K^{(*)}\psi^{(\prime)}$ followed by $\psi^{(\prime)} \to \ell^+\ell^-$ and from $c\bar{c}$ continuum intermediate states. The short distance contributions lead to the inclusive branching fractions $B(B \to X_s \ell^+ \ell^-) = (15, 7, 2) \times 10^{-6}$ for $\ell = e, \mu, \tau$, and will likely be observed before PEP-II is operational. However, the best method of separating the long and short distance contributions, and observing any small deviations from the Standard Model, is to measure the various kinematic distributions associated with the final-state lepton pair, such as the lepton pair invariant mass distribution, the lepton pair forward-backward asymmetry, and the tau polarization asymmetry. Measurement of these distributions requires the high statistics samples available at PEP-II. Here, the long-distance contributions dominate only in the $m(\ell^+\ell^-)$ regions near the J/ψ and ψ' resonances, and observations away from these peaks cleanly separate the short distance physics. The values of the forward-backward and tau polarization asymmetries are large for currently favored values of the top quark mass around $175\,\mathrm{GeV}/c^2$ [Abe94]. Measurement of all three kinematic distributions would provide a unique determination of the sign and magnitude of each contributing short distance operator, and hence, would provide a stringent test of the Standard Model.

3.10.3 $B \to X_s \nu\bar{\nu}$

The decay $B \to X_s \nu\bar{\nu}$ proceeds through Z^0-penguin and W-box diagrams yielding an inclusive branching fraction of 5×10^{-5}. Measurement of this process would help to determine the size of Z^0-penguin effects in rare B hadronic decays, such as $B \to \pi\pi$. A search for such decays will focus on events with large missing E_T opposite a reconstructed B. High integrated luminosity, good detector hermeticity, and efficient K_L identification for background rejection are important for this mode. The search will require at least 10^5 reconstructed B mesons. The reduction in continuum background problems offered by the separate vertexing of the two Bs in an event will be a significant advantage for this channel.

3.11 *CP* Asymmetries in Charged B Decays

CP asymmetries in charged B decays are another important and as-yet-unexplored region of physics. While these asymmetries offer no direct measurement of CKM parameters, unlike the neutral B case, their observation is nonetheless essential to our full understanding of the physics of B decays. Any observed asymmetry in charged B decays is a direct *CP*-violation effect and would, for example, rule out the superweak alternative theory of *CP* violation. These asymmetries require interference between two amplitude contributions that have both different weak phases and different strong phases. In the Standard Model they are expected to be largest in a channel such as $K\pi$ in which tree amplitudes are CKM suppressed relative to penguin contributions, and hence the relative strengths of the two types of terms are comparable. Unknown strong phases make even this statement a crude estimate rather than a rigorous prediction. However, if factorization proves to be a good approximation, then, within the Standard Model, this expectation for $K\pi$ becomes quite reliable. Of course, the total rate for such a channel is also suppressed, so it remains to be seen whether it will be easier to measure a small asymmetry in a relatively high rate channel or a larger asymmetry in a rare decay mode.

There are aspects of detector design of particular importance. Just as with the neutral channels, issues such as particle identification for distinguishing $K^{\pm}\pi^0$ from $\pi^{\pm}\pi^0$ decays, are crucial to any such search. Clearly, one also needs to be able to detect π^0s and other calorimeter signatures to perform such studies. Likewise, good detector resolution is needed to allow cuts that eliminate light-quark-produced backgrounds without excessive deterioration in signal. Thus, a detector designed to perform well in the neutral B case is also well-adapted for a study of charged B decays and a search for possible *CP*-violating effects in these channels.

3.12 Charm Physics

BaBar's expected high D meson production rates, good time resolution between decays, particle identification systems, and near hermetic efficiency should make high sensitivity searches into $D\overline{D}$ mixing, rare decay physics, and *CP* violation in the charm sector feasible.

3.12.1 $D^0\overline{D}^0$ Mixing

Within the Standard Model, $D^0\overline{D}^0$ mixing is expected to be very small. The amount of mixing is governed by $x_{mix} = \Delta m/\Gamma$ and $y_{mix} = \Delta\Gamma/\Gamma$, where Δm is the mass difference between $D^0 - \overline{D}^0$ states, and Γ is the decay rate. In the Standard Model, estimates for x_{mix} and y_{mix} are in the range 10^{-3}–10^{-5} [Liu94]. If mixing is enhanced, this would be a sign of new physics. Unless the $D\overline{D}$ mixing rate is exceptionally large, it will not be significantly tested in the near future. *BaBar* can play an important role in placing a limit on the experimental sensitivity of $D\overline{D}$ mixing at about $x_{mix} \sim 10^{-2} - 10^{-3}$, a range of interest for some nonstandard model predictions [Hal92].

The experimental limitations on mixing sensitivity come primarily from two sources, doubly-Cabibbo-suppressed decays (DCSD), which mimic mixing in pure hadronic channels, and experimental backgrounds. The mixing term behaves as $\sin(\Delta mt)$. Thus, with small x_{mix}, one looks for mixing with optimum sensitivity at or beyond two decay lifetimes. Even after a few lifetimes, one is sensitive to fluctuations in the tails of the DCSD rate. In addition, experimental backgrounds can result from combinatorial counting, poor vertex reconstruction, particle misidentification, and confusion with other long-lived decay products. Such backgrounds can be reduced by vertex separation cuts, particle identification requirements, and rejection of mass reflections, *etc.*

Either resonant or continuum production of D^*s can be used for mixing studies in *BaBar*. Commonly used decay chains such as $D^{*+} \to D^0\pi^+$, then $D^0 \to K^-\pi^+$, $K^-\pi^-\pi^+\pi^-$, $K^-l\overline{\nu}$, and even $K^-\pi^+\pi^0$, require measurement of the sign of the π from the D^* decay to define the initial D^0 flavor. In the boosted system of *BaBar*, this π usually has enough momentum to be reconstructed with high efficiency. The good particle identification properties of *BaBar* are important in analyzing such channels. The *BaBar* vertex detector will have adequate proper time resolution to resolve the decay time development of the DCSD from that of decay after mixing.

With sufficiently high statistics samples, searches via semileptonic decays may ultimately provide better mixing limits. Semileptonic decay channels have no DCSD contributions, but experimental backgrounds due to incomplete reconstruction of the fully leptonic final state can dominate the measurement error.

3.12.2 *CP* Violation in Charm Decays

CP-violating effects are also predicted to be very small in the charm sector, although some have argued that they may be significantly enhanced without requiring physics beyond the Standard Model [Gol89, Buc93]. Again, with high reconstruction efficiencies for charm decays and efficient tagging mechanisms, *BaBar* will be sensitive to observation of *CP*-violating effects in the charm sector.

In order for *CP* violation to occur, there must exist two transition amplitudes to a final-state f which interfere with nonzero relative phase. In the Standard Model, neutral D decay *CP*-violating asymmetries from mixing are suppressed by the low mixing rate and are not expected to be seen. However, direct *CP*-violating effects in Cabibbo-suppressed modes, due to interference between the suppressed tree amplitude and an unsuppressed penguin amplitude, may be as high as a few times 10^{-3} [Buc93, Fry93]. Strong candidates for searches include $D^+ \to \overline{K}^{*0}K^+$, $D_s^+ \to K^{*+}\eta'$ decays, and $D^0 \to K^+K^-$. Limits set by current experiments [Fra94] have not tested the $A_{CP} \sim 10^{-3}$ range, and *BaBar* should be able to make major contributions.

3.13 Tau Physics

Tau physics is now precision physics. There are no longer any obvious discrepancies between experimental tau physics and Standard Model predictions: lepton universality has been confirmed to better than 1%; world average exclusive branching fractions sum to within 1% of 100%. Further progress in tau physics will come from high precision, detailed studies of both leptonic and semihadronic tau decays, studies of tau spin structure, and searches for rare or forbidden decays. Taus are still a rich field of physics, and the potential still exists for uncovering physics beyond the Standard Model.

The cross section for tau pairs at $E_{cm} = 10.58\,\text{GeV}$ is 0.91 nb, so an integrated luminosity sample of $30\,\text{fb}^{-1}$ will contain 27×10^6 tau pairs. (The current total world sample is on the order of 6×10^6 tau pairs, dominated by CLEO.) With such a large sample, significant contributions can be made to all of the topics discussed below. Many studies will be dominated by systematic errors, so it is important to critically evaluate the strengths and weaknesses of *BaBar* for addressing these issues.

Tau physics is more difficult at *BaBar*, than at LEP because: at *BaBar* there will be significant backgrounds from $q\overline{q}$ events and two-photon physics, which require relatively hard, mode-dependent cuts to isolate a signal; π^0s are softer and therefore more difficult to detect reliably; and electrons and muons are softer and are thus more difficult to distinguish from pions. However, the extremely large data sample will make it possible to trade statistics for systematics, for example, in the use of clean tags such as $\tau \to e\nu\nu$, so that improved systematic errors can be achieved. More importantly, the scope of interesting physics goals will be more focused; *BaBar* will concentrate on some important measurements that can be done very well with its large data sample. Some of the topics that will be of interest in the twenty-first century, to which *BaBar* can make a significant contribution, are discussed below.

- Second-class currents (which violate isospin) have not yet been observed in tau decay. The decay $\tau^- \to \eta\pi^-\nu_\tau$ is predicted to proceed at the 10^{-5} level. The decay $\tau^- \to \omega\pi^-\nu_\tau$ occurs predominantly through the vector current; the decay via the axial-vector current, which violates isospin, can be observed by analyzing the angular distribution.
- Detailed studies of tau decays to three pseudoscalar mesons ($\pi\pi\pi\nu_\tau$, $K\pi\pi\nu_\tau$, and $KK\pi\nu_\tau$) will yield information on the Weiss-Zumino anomaly, isospin violation, $SU(3)_f$ breaking, K_1 mixing, and other aspects of these hadronic currents.
- Detailed studies of the spectral functions in decays to $3\pi\nu_\tau$, $4\pi\nu_\tau$, $5\pi\nu_\tau$, and $6\pi\nu_\tau$, in comparison with data from e^+e^- annihilation, permit precise tests of CVC and PCAC.

- Studies of the spectral functions, carefully separated into vector and axial vector components, and strange and nonstrange components, permit tests of Weinberg, DMO, and other sum rules.

- Precision measurements of the Michel parameters ρ, η, ξ, and δ in leptonic tau decays and of the parity-violating neutrino helicity in semihadronic decays test the V–A Lorentz structure of the $\tau - W^- - \nu_\tau$ coupling, and are thus sensitive to the presence of scalar (charged Higgs) or V+A (W_R) currents. The spin-dependent Michel parameters ξ and δ can be measured by exploiting the well-understood (in QCD) correlations between tau spins in e^+e^- annihilation through the analysis of momentum and angle correlations between the decay products of the two taus in the event.

- One can search for *CP* violation in the leptonic sector in a variety of ways. A nonzero electric dipole moment will increase the total $e^+e^- \to \tau^+\tau^-$ cross section and angular distribution and affect the energy distribution of the π^- in the decay $\tau^- \to \pi^-\nu_\tau$. It will also produce nonzero expectation values for *CP*-odd correlation tensors between the decay products of the two taus in the event.

- In tau decays, final states containing no neutrinos violate lepton family number. Limits on branching fractions for these processes are at the few 10^{-6} level. Some models, with massive Majorana neutrinos or mass-dependent couplings, predict branching ratios near this level. It is thus of interest to push these limits down by another order of magnitude.

- The current best direct bound on the tau neutrino mass is around $25\,\mathrm{MeV}/c^2$. Constraints from Big Bang nucleosynthesis and SN-1987A exclude long-lived Dirac tau neutrinos below 15 keV. However, if the tau neutrino has a mass between 1 and $25\,\mathrm{MeV}/c^2$ and a lifetime in the range 10^3–10^6 seconds, it can evade nucleosynthesis bounds, contribute to dark matter, and help explain how type II supernovae explode. It is thus of great interest to search for a tau neutrino mass in this range.

3.14 Two-Photon Physics

Monte Carlo studies [Bau92] have shown that a high-luminosity *B* Factory will extend the study of exclusive two-photon physics from the present $2\,\mathrm{GeV}/c^2$ up to at least $5\,\mathrm{GeV}/c^2$ in mass. This will likely reveal many of the exotic bound-states now being sought, such as glueballs, $q\bar{q}g$ hybrids, and four-quark resonances. Measurements of the two-photon couplings of light quark and charmonium resonances will continue to be very important for understanding quark dynamics. Furthermore, a real challenge to perturbative QCD predictions of exclusive hadron production from two-photon interactions can be made by

Untagged Reactions	Published Data	Expected B Factory ($100\,\mathrm{fb}^{-1}$)
$\gamma\gamma \to \eta' \to \pi^+\pi^-\gamma$	2000	300,000
$\gamma\gamma \to \iota(1.42\ \mathrm{GeV}) \to \overline{K}K\pi$	0	600
$\gamma\gamma \to \eta_c \to$ all modes	10	30000
$\gamma\gamma \to \pi^+\pi^-$ (W > 3 GeV)	10	800

Single-Tagged Reactions	Published Data	Expected B Factory ($100\,\mathrm{fb}^{-1}$)
$\gamma\gamma* \to \eta' \to \pi^+\pi^-\gamma$	300	6000
$\gamma\gamma* \to 1^{++}(1.42\,\mathrm{GeV}/c^2) \to \overline{K}K\pi$	30	1100
$\gamma\gamma* \to \eta_c \to$ all modes	1	3000
$\gamma\gamma* \to \pi^+\pi^-$ (W > $3\,\mathrm{GeV}/c^2$)	—	100

Table 3-20. *Comparison of current published event samples for two-photon physics with the number of events expected at BABAR with $100\,fb^{-1}$ of luminosity.*

obtaining statistics in the $> 3\,\mathrm{GeV}/c^2$ mass range. Finally, there is a strong incentive to study single-tagged two-photon reactions (where one of the scattered $e^{\pm}$s is detected) since, when one of the photons is far from the mass shell, spin-1 resonances can be isolated (especially $J^{PC} = 1^{-+}$ $q\overline{q}g$ hybrid states) and unique QCD predictions can be tested.

Table 3-20 summarizes Monte Carlo event rate predictions for $100\,\mathrm{fb}^{-1}$ of data at PEP-II, along with present world average data samples. Clearly, at least a factor of 30 improvement in statistics can be made in all of these exclusive processes. Furthermore, new channels will be available, with a high-quality detector, which have not been explored in the past. Most of this can be accomplished with little impact on the optimal detector for studying *CP* violation. The main requirement is a very flexible trigger which can allow detection of low-mass and low-multiplicity final states with balanced transverse momenta. However, study of the single-tagged reactions require detection of low-angle scattered positrons in the backward direction down to polar angles of 300 mr. Those topics will need to wait for a detector upgrade which adds a backward calorimeter.

3.15 Summary

The variety of physics accessible at PEP-II demands a general-purpose detector, as is typical in colliding beam experiments. The detector discussed here has been optimized for *CP*-violation studies. However, since so many modes contribute to such studies, this process automatically leads to a detector which can address a much wider range of physics issues. The set of topics presented in this chapter is in no way intended to be an exhaustive list of all the physics studies possible with this detector, but rather an overview showing that a rich program is expected. The *BaBar* detector will undertake all possible aspects of this program.

References

[Abe94] F. Abe *et al., Phys. Rev. Lett.* **73**, 2667 (1994).

[Alb94*b*] H. Albrecht *et al.* (ARGUS Collaboration), *Z. Phys.* **C62**, 371 (1994).

[Ale91] R. Aleksan, I. Dunietz, B. Kayser, and F. LeDiberder, *Nucl. Phys.* **B361**, 161 (1991).

[Ale92] R. Aleksan, A. Gaidot, and G. Vasseur, "Probing the Penguin Contribution in $B \to \pi\pi$ at an Asymmetric B Meson Factory," DAPNIA/SPP 92–19 (1992).

[Ale93] R. Aleksan, L. Oliver, O. Pene, and J.C. Raynal, *Phys. Lett.* **B317**, 123 (1993).

[Atw94] D. Atwood, B. Blok, and A. Soni, SLAC–PUB–6635 (1994).

[Bar90] V. Barger, C.S. Kim, and R.J.N. Phillips, *Phys. Lett.* **B251**, 629 (1990).

[Bat93a] M. Battle *et al., Phys. Rev. Lett.* **71**, 3922 (1993).

[Bau92] D.A. Bauer, SLAC–400, 608 (1992); also SLAC–373, 173 (1992).

[Bro93] T.E. Browder *et al.,* "A Review of Hadronic and Rare B Decays," CLNS 93/1261 (1993).

[Bro95] T.E. Browder and S. Pakvasa, University of Hawaii Report UH–511–814–95 (1995).

[Buc93] F. Buccella *et al., Phys. Lett.* **B302**, 319 (1993).

[CER93] GEANT Detector Description and Simulation Tool, Version 3.15, CERN Program Library W5103, CERN (1993).

[Cha95] J. Chauveau and P. David, "Reconstruction of the Vertex in Lepton-tagged B Mesons," *BaBar Note* # 224 (1995).

[Cou95] D. Coupal, "Study of $B^0 \to D^+D^-$ and $B^0 \to D^{*+}D^{*-}$ in BaBar," *BaBar Note* # 211 (1995).

[Dea93] A. Deandrea, N. Di Bartolomeo, R. Gatto, and G. Nardulli, *Phys. Lett.* **B318**, 549 (1993).

[Des94] N.G. Deshpande, X.G. He, and J. Trampetic, University of Oregon Report OITS–564 (1994).

[Des95] N.G. Deshpande and X.G. He, *Phys. Rev. Lett.* **74**, 26 (1995).

[Fra94] P.L. Frabetti *et al., Phys. Rev.* **D50**, 2953 (1994).

[Fry93] J.R. Fry and T. Ruf, "Prospects of Studying *CP* Violation and Mixing in D Decays at a τ-charm Factory," Third Workshop on the τ-charm Factory, Marbella, Spain (1993).

[Gol89] M. Golden and B. Grinstein, *Phys. Lett.* **B222**, 501 (1989).

[Gol94] E. Golowich and S. Pakvasa, University of Massachusetts Report UMHEP-411 (1994).

[Gro90] M. Gronau and D. London, *Phys. Rev. Lett.* **65**, 3381 (1990).

[Hal92] L. Hall and S. Weinberg, *Phys. Rev.* **D48**, 979 (1992).

[Har95] P. Harrison, "Study of $B \to J/\psi K^0_s$, $J/\psi K^*$ and $\rho\pi$," *BaBar Note* # 218 (1995).

[Inn93] W. Innes, "TRACKERR, A Program for Calculating Tracking Errors," *BaBar Note* # 121 (1993).

[Jad90] S. Jadach and Z. Was, "KORALB 2.1: An Upgrade with Tauola Library of Tau Decays," Comput. Phys. Comm. **64**, 267 (1991).

[Jaf94] D.E. Jaffe, F. Le Diberder, M.H. Schune, and G. Wormser, "Treatment of Weighted Events in a Likelihood Analysis of B_s Oscillations or *CP* Violation," *BaBar Note* # 132 (1994).

[Liu94] T. Liu, "The Future of High-Sensitivity Charm Experiments," in Proceedings of the CHARM2000 Workshop, edited by D. Kaplan and S. Kwan (Fermilab, Batavia, Illinois), pp 7–9 (1994).

[Nir93] For a Review of Standard Model Predictions on *CP* Violation in B Decays see Y. Nir and H.R. Quinn, *Ann. Rev. Nucl. Sci.* **42**, 211 (1992), and references contained therein.

[PDG94] L. Montanet *et al.* (Particle Data Group), *Phys. Rev.* **D50** (1994).

[Pia94] M.G. Pia, "B Tagging with Muons," *BaBar Note* # 192 (1994).

[Pla95] S. Plaszczynski, M.-H. Schune, and G. Wormser, "An Improved Tagging for the *BaBar* Experiment," *BaBar Note* # 209 (1995).

[Qui93] H.R. Quinn and A. Snyder, *Phys. Rev.* **D48**, 2139 (1993).

[Ric95] J.D. Richman and P.R. Burchat, "Lepton and Semileptonic Decays of Charm and Bottom Hadrons," submitted to *Rev. of Mod. Phys.*

[Sjo93] T. Sjöstrand, "PYTHIA 5.7 and JETSET 7.4 Physics and Manual," CERN–TH 7112/93 (1993).

[SLA89] For earlier studies see SLAC–353 (1989), SLAC–400 (1992), and SLAC–419 (1993).

[Sjo93] T. Sjostrand, "JETSET 7.4," CERN-TH 7111/93, (1993).

[Sny90] A. Snyder and S. Wagner, "An Alternate Method of B-Tagging for *CP* Violation Studies," *BaBar Note* # 25 (1990).

[Sny94] A. Snyder, "*CP* Extraction Tool," *BaBar Note* # 188 (1994).

[Sny95] A. Snyder, "*CP* Reach Calculation of the TDR," *BaBar Note* # 219 (1995).

[Wal94*a*] R. Waldi, "Flavor Tagging of B^0 Decays: Using All Available Information," *BaBar Note* # 190 (1994).

[Wal95] R. Waldi, "Flavor Tagging Studies for the *BaBar* TDR," *BaBar Note* # 204 (1995).

[Wea95] M. Weaver, "Tag Mode Vertex Resolution Studies," *BaBar Note* # 227 (1995).

[Wol85] L. Wolfenstein, *Phys. Rev.* **D3**, 2381 (1985).

[Wri94a] D. Wright, "BEGET: The B Factory Event Generator," *BaBar Note* # 149 (1994).

[Wri94b] D. Wright, "K_L^0 identification in $B^0 \rightarrow J/\psi K_L^0$ Decays," *BaBar Note* # 201 (1994).